
This manuscript is a non-peer reviewed preprint uploaded to EarthArXiv. The manuscript has been submitted for publication to The Depositional Record. Please feel free to contact any of the authors; we welcome feedback.

1 **Internal mouth bar variability and preservation of interflood beds in low-accommodation**
2 **proximal deltaic settings (Cretaceous Dakota Group, New Mexico, USA)**

3
4 Anna E. van Yperen¹, Miquel Poyatos-Moré¹, John M. Holbrook², & Ivar Midtkandal¹

5
6 ¹University of Oslo, Department of Geosciences, P.O. Box 1047 Blindern, 0316 Oslo, Norway

7 ²Texas Christian University, Department of Geological Sciences, TCU Box 298830, Fort Worth, Texas 76129

8 Corresponding author: annavanyperen@gmail.com

9
10
11 **ABSTRACT**

12 Mouth bars are the fundamental architectural elements of proximal deltaic successions. Understanding
13 their internal architecture and deciphering the relative impact and complex interaction of coastal
14 processes (fluvial-, tide- and wave-dominated) is paramount to the interpretation of ancient deltaic
15 successions. This is particularly challenging in low-accommodation systems, because they are commonly
16 characterized by thin, condensed and top-truncated sections. In this study, we analyze the exhumed
17 Cenomanian Mesa Rica Sandstone (Dakota Group, Western Interior Seaway, USA), which encompasses a
18 fluvio-deltaic system covering a ~450 km profile oriented parallel to depositional-dip direction. The
19 study targets the proximal deltaic expression of the system, with 22 sedimentary logs (total of 390 m)
20 spatially correlated within a ~25 km² study area at the rim of the Tucumcari Basin. Analysis of facies
21 distributions, depositional architecture and spatial extent of stratigraphic surfaces reveals a 6–10-m-
22 thick, sharp-based and sand-prone deltaic package, comprising several laterally-extensive (>800 m width)
23 mouth bars. Composite erosional surfaces infilled with multi-story fluvial and marine-influenced channel
24 deposits (12–20 m thick, 100–250 m wide) scour locally into the deltaic package. Based on differences in
25 sedimentary structures, bed thicknesses, occurrence of interflood beds and bioturbation indexes, we
26 distinguish four different subenvironments within single mouth bars. These range from mouth bar axis,
27 off-axis, fringe to distal fringe deposits, and each reflect differences in hydraulic conditions as moving
28 away from the main active feeding channel. The interpreted mouth bar components also show intra-
29 mouth-bar variability in dominant process regime, with overall river dominance but local preservation of
30 tide influence in the fringe and distal fringe components. Mouth bar deposits amalgamate to form an
31 extensive sand-rich sheet body throughout the study area, in which interflood mudstone to very-fine
32 grained sandstone beds are nearly absent. These features are interpreted to reflect successive
33 coalescence of mouth bars in a low accommodation / supply (A/S) setting. These conditions promoted

34 channel avulsion/bifurcation and thus the potential reworking of previously deposited mouth bar fringe
35 and distal fringe sediments, where tide influence tends to be better recorded. Results of this study
36 evidence a common mixed nature and internal process-regime variability within mouth bar components.
37 They also caution against the possible loss of preservation of subordinate processes (e.g. tidal indicators),
38 and consequent underestimation of the true mixed influence in low-accommodation deltaic settings.

39

40 Key words: low accommodation, mouth bar, delta, interflood beds, preservation, Dakota Group

41

42

INTRODUCTION

43 Mouth bars are fundamental architectural elements of proximal deltaic successions. They form at the
44 river mouth, where flows confined within a distributary channel expand and decelerate as they enter a
45 standing body of water (Bates, 1953; Wright, 1977; Elliott, 1986). The plan-view, cross-sectional
46 geometry and scale of mouth bars is controlled by the relative dominance of coastal processes,
47 influencing their shape and typical aspect ratio (length: width) (e.g. Wright, 1977; Postma, 1990;
48 Bhattacharya, 2006; Gani and Bhattacharya, 2007). Additionally, increased bedload and/or shallower
49 receiving water depths result in broad mouth bar deposits, as enhanced effects of bed friction cause
50 more rapid spatial expansion and deceleration of the river jet (Wright, 1977). Mouth bar depositional
51 cycles consist of deposition, extension, avulsion and abandonment (Olariu and Bhattacharya, 2006).
52 Numerical modeling suggest that individual mouth bars prograde until the water depth over the bar is
53 equal to or less than 40% of the inlet depth, after which aggradation becomes dominant (Edmonds and
54 Slingerland, 2007). This decreases distributary channel discharge and forces its bifurcation (Olariu and
55 Bhattacharya, 2006; Edmonds and Slingerland, 2007) or avulsion (e.g. Bhattacharya, 2010). Both options
56 lead to the initiation of new mouth bar deposition, and they are enhanced in high sediment supply and
57 low accommodation conditions (Van Yperen et al., *in press JSR*).

58 Mouth bars consist of beds and bedsets that reflect flood and interflood deposition related to seasonal
59 variations in flow conditions and sediment input (Dalrymple et al., 2015; Gugliotta et al., 2016a). Finer-
60 grained facies (i.e., 'interflood beds') deposit during times of low energy between river flood periods,
61 whereas 'river flood beds' are thicker and consist of coarser-grained facies deposited during times of
62 high river discharge (Dalrymple et al., 2015; Gugliotta et al., 2016a). River flood beds are amalgamated
63 towards the top and are dominant in the proximal part of mouth bars, whereas interflood beds occur
64 predominantly at mouth bar fringes (Fig. 1) (Gugliotta et al., 2016a). If not obscured by bioturbation, and
65 if deposition takes place within a tide-influenced zone, these interflood beds can show tidal rhythmites,

66 double mud drapes, and/or bidirectional current ripples (Dalrymple et al., 2015, and references therein).
67 If a depositional system or zone experiences only weak tidal energy, tidal indicators have highest
68 preservation potential in the interflood beds (e.g. Gugliotta et al., 2016b; Kurcinka et al., 2018). These
69 interflood beds represent more time than the flood deposits (e.g. Miall, 2015).

70 Beds and bedsets within mouth bars represent basinward-accreting bar-front surfaces (e.g. Gani and
71 Bhattacharya, 2007) emanating from a relatively fixed distributary channel mouth (Wellner et al., 2005).
72 Individual mouth bars coalesce and stack compensationally to form mouth bar complexes (Fig. 2) (e.g.
73 Wellner et al., 2005; Enge et al., 2010). Mouth bar complexes are related to the same progradation
74 pulse (Ainsworth et al., 2016) and their distributary channel network is genetically linked (Wellner et al.,
75 2005). Delta lobes consist of mouth bar complexes related to the same primary distributary feeder
76 channel; new lobes form when the channel avulses or erodes through the delta lobe and initiates new,
77 larger-scale mouth bar deposits outside the stranded lobe (Ainsworth et al., 2016). At both mouth bar
78 complex and delta lobe scale, individual mouth bars typically become smaller and finer-grained as the
79 distributary channel network progrades (Wellner et al., 2005). The amalgamation of mouth bars into
80 mouth bar complexes and delta lobes is the building mechanism for deltas, and avulsion and/or
81 bifurcation are the driving forces for their lateral development (Edmonds and Slingerland 2007).

82 Internal differentiation of individual mouth bars is executed but not common in ancient deltaic
83 successions (e.g. Olariu and Bhattacharya, 2006; Gani and Bhattacharya, 2007; Enge et al., 2010; Jerrett
84 et al., 2016; Fidolini and Ghinassi, 2016). In deep-water sedimentology it is common to differentiate
85 submarine fan lobe deposits internally and distinguish lobe axis, off-axis, fringe and distal fringe sub-
86 environments (e.g. Hodgson, 2009; Pr elat et al., 2009; Hofstra et al., 2016; Sychala et al., 2017). A
87 similar subdivision in ancient mouth bar deposits is uncommon but differentiation between axial and
88 fringe deposits has been made (e.g. Jerrett et al., 2016; Fidolini and Ghinassi, 2016). Detailed work on
89 modern deltas shows predictable grainsize and bedform trends within individual mouth bar deposits
90 (e.g. Wellner et al., 2005). These are all consistent with an overall waning flow lithofacies association in
91 all directions away from the central axis.

92 In this study, we analyze the proximal deltaic expression of the exhumed Cenomanian Mesa Rica
93 Sandstone (Dakota Group, Western Interior Seaway, USA), with the aim to: i) describe and analyse the
94 spatial distribution of sedimentary facies and stratigraphic architecture of its proximal deltaic expression;
95 ii) distinguish and discuss different processes and deposits from internal mouth bar components; and iii)
96 discuss the role of low-accommodation conditions in resulting deltaic geometries and preservation
97 potential of interflood deposits.

GEOLOGICAL SETTING AND STRATIGRAPHIC FRAMEWORK

100 The Mesa Rica Sandstone (hereafter referred to as 'Mesa Rica') was deposited ~98-99 Ma during the
101 Cenomanian (Scott et al., 2018) and is the oldest formation within the Dakota Group in Colorado and
102 New Mexico (e.g. Holbrook and Wright Dunbar, 1992; Scott et al., 2004). The Dakota Group is among the
103 eastward prograding sedimentary systems of the US Western Interior that were sourced from the Sevier
104 fold-and-thrust belt (e.g. MacKenzie and Poole, 1962; Dickinson, 2018 and references herein, Van
105 Yperen et al., *in press NMGS*). The latter formed during the Cordilleran orogeny, with subduction of the
106 Farallon plate beneath the west coast of North America causing back-arc compression in the Late
107 Jurassic (DeCelles, 2004). The Dakota Group also received minor sediment volumes from other smaller
108 topographic highs (Kisucky, 1987; Holbrook and Wright Dunbar, 1992). The study area is located at the
109 northwestern rim of the Tukumcari Basin (Fig. 3A), which formed during the late Carboniferous and early
110 Permian as a tectonic element of the Ancestral Rocky Mountains (Broadhead, 2004).

111 An overall NW to SSE-directed depositional profile characterizes the Dakota Group in southeastern
112 Colorado and northeastern New Mexico. The Dakota Group is further subdivided into the Mesa Rica,
113 Pajarito (Dry Creek Canyon member in south-central Colorado and northeastern New Mexico) and
114 Romeroville formations. These represent phases of predominantly fluvial, paralic, and fluvial deposition,
115 respectively (Fig. 3B). Regional sequence boundary SB3.1 (Fig. 3B) forms the base of the Mesa Rica and
116 relates to a late Albian – early Cenomanian forced-regression, which caused widespread erosion in
117 southeast Colorado and northeast New Mexico (Holbrook and Wright Dunbar, 1992; Holbrook, 1996;
118 Holbrook, 2001; Scott et al., 2004; Oboh-Ikuenobe et al., 2008). In east-central New Mexico, only the
119 Mesa Rica and Pajarito formations are preserved, and the former can be in turn subdivided into the
120 lower, middle, and upper Mesa Rica (Scott et al., 2004; Van Yperen et al., *in press NMGS*). This
121 subdivision relates to depositional transgression-regression (T-R) cycles and record higher-frequency
122 relative sea-level fluctuations in the Western Interior Seaway (e.g. Holbrook and Wright Dunbar 1992;
123 Holbrook 1996; Scott et al., 2004; Oboh-Ikuenobe et al., 2008). In the Tukumcari Basin, the open marine
124 Albian-Cenomanian Tukumcari Shale separates the fluvial Jurassic Morrison Formation from the fluvio-
125 deltaic, Cretaceous Dakota Group (Fig. 3B) (e.g. Holbrook and Wright Dunbar 1992; Scott et al., 2004;
126 Van Yperen et al., *in press JSR*). The Tukumcari Shale is locally underlain by estuarine deposits of the
127 informally defined Cretaceous Campana Sandstone Bed (hereafter referred to as "Campana") (Holbrook
128 et al., 1987; Holbrook and Wright Dunbar, 1992). This represents the sandy infill of local topographic

129 lows, as the Late Jurassic landscape was progressively inundated during relative sea-level rise (Holbrook
130 et al., 1987).

131 The lower Mesa Rica shows a change from fluvial to deltaic deposits at the northwestern rim of the
132 Tucumcari Basin, which reflects the most proximal shallow-marine deposition within the Mesa Rica
133 depositional system (Holbrook and Wright Dunbar, 1992; Van Yperen et al., *in press NMGS*). Upstream,
134 time-equivalent fluvial strata record deposition of a >80 km-wide single-story channel sheet (e.g.
135 Holbrook, 2001). Downstream, in the center of the Tucumcari Basin, coalesced mouth bars consistently
136 overlain by sand-filled amalgamated distributary channels characterize the contemporaneous deltaic
137 deposits (Van Yperen et al., *in press JSR*). The upper Mesa Rica represents a lower delta plain
138 environment with fluvial distributary channel deposits (e.g. Scott et al., 2004; Holbrook et al., 2006; Van
139 Yperen et al., *in press NMGS*) and an increased presence of marine-influenced distributary channel
140 deposits towards the center of the basin (Van Yperen et al., *in press JSR*).

141 During the Cretaceous, the study area was located at $\sim 35^{\circ}$ N latitude, with a prevailing warm and humid
142 climate (Chumakov et al., 1995).

143

144

METHODS AND DATA

145 The field study focused on the lower Mesa Rica, which is deltaic in the study area, because the main
146 objective of this work is the recognition of internal architecture of ancient deltaic sandstone bodies.
147 However, the upper Mesa Rica and the stratigraphic relationships with underlying and overlying strata
148 are also briefly reported in the results below.

149 Stratigraphic sections were measured at 1:100 cm scale (18 logs) and 1:200 cm scale (4 sketch logs)
150 within a ~ 25 km² area, at the Trigg Ranch in San Miguel County, east-central New Mexico (Fig. 4).
151 Sedimentary facies analysis was based on lithology, texture, sedimentary structures, and bioturbation
152 assemblage and intensity. The latter was recorded using the 1–6 bioturbation index (BI) scheme of
153 Taylor and Goldring (1993). UAV (unmanned aerial vehicle) imagery (shot with a Phantom 4 Pro ®),
154 photomontages, and field sketches are used to map sedimentary body geometries, lateral distributions,
155 architectural elements and extension of key stratigraphic surfaces. These form the basis of a fence
156 correlation diagram that correlates constructed depositional-dip ($\sim 6,5$ km) and strike-oriented (~ 4 km)
157 panels. Paleocurrent measurements (N=260) were obtained from cross-stratification and cross-
158 lamination foresets.

159

160

FACIES ANALYSIS

161 The studied strata are divided into 13 facies (f1–13) based on observations of lithology, grain size,
162 sedimentary structures, paleocurrents, bioturbation indices, and interpreted depositional processes
163 (Table 1, Figs. 5–9). We grouped the facies into nine facies associations (FA1–9) that reflect different
164 environments of deposition, based on the combination of dominant sedimentary processes (facies),
165 bioturbation intensity, and lateral and vertical facies relationships.

166

167

FA1 – Prodelta

168 **Description** - Gray, structureless muddy siltstone (f1, Table 1) found in sharp contact with overlying
169 delta front deposits (FA2-FA5). FA1 thicknesses average 0.3–0.7 m (max. 2 m thick). Bioturbation indices
170 are high (BI 4–5) and we identified *Thalassinoides*, *Phycosiphon*, *Planolites*, *Teichichnus*, *Chondrites*, and
171 *Helminthopsis* (Fig. 7A). Macrofauna was not observed.

172 **Interpretation** - Deposition occurred below fair-weather wave base, in a low-energy setting beyond the
173 influence of the river effluent (e.g. Wright and Coleman, 1973; Gani et al., 2009). The stratigraphic
174 position of FA1 relates to the open marine Tucumcari Shale, with abundant macrofauna (e.g.
175 *Texigrapheya*, *Peilina levicostata*) within the Tucumcari Basin (e.g. Scott, 1974; Holbrook and Wright
176 Dunbar, 1992; Kues, 1997; Oboh-Ikuenobe et al., 2008). In the study area however, a shallower setting is
177 inferred from the thin and silty appearance and lack of macrofauna indicative of open marine settings
178 (e.g. Holbrook et al., 1987; Kisucky, 1987; Holbrook and White, 1998). The trace fossils indicate brackish
179 to normal marine conditions (MacEachern and Bann, 2008).

180

181

FA2 – Mouth bar axis

182 **Description** – FA2 consists of two subsets: FA2.a consists of laterally-extensive sandstone beds with a
183 tabular, sharp-bedded nature and display an alternation of f2 with f3, f4 and/or f5 (Fig. 8A, Table
184 1). Facies f2 consists of 10–30-cm-thick poorly-sorted, clast supported conglomerate beds with common
185 (faint) stratification (Fig. 5A). Facies f3 consists predominantly of 30–50-cm-thick fine-grained
186 structureless sandstone beds, and rare planar lamination (f4) and cross-stratification (f5). The contact
187 surface between the alternating facies is sharp or gradational. Conglomerate beds become increasingly
188 amalgamated upwards and grade into better sorted, through- and tangential cross-stratified pebbly
189 sandstone (f6, Fig. 5B, Table 1). *Ophiomorpha* trace fossils (BI 0–2) occur predominantly in the upper
190 part of the structureless sandstone beds (Fig.7B). FA2.b consists of 40–60-cm-thick cross-stratified (f5)

191 and parallel-laminated (f4) sandstone, with common soft-sediment deformation and an absence of mud.
192 In places, dispersed granules occur in cross-stratified sandstone beds.

193 FA2 units are 8–10 m thick, reveal arrangement in ~8° dipping accretionary strata in places, and grade
194 laterally into FA3 (mouth bar – off-axis). FA2 is locally eroded and overlain by FA6 (distributary channel
195 deposits).

196 **Interpretation** – FA2 deposits are associated with high-energy deposition close to the river mouth (e.g.
197 Wright, 1977; Enge et al., 2010; Fidolini and Ghinassi, 2016). We interpret FA2.a as hyperpycnites (*sensu*
198 Mulder et al., 2003) because of their position in the sedimentary system, grain size, and trends in
199 sedimentary structures. The latter show an alternation of different conforming facies that reflect
200 repetitive deposition from different flow types and represent deposition dominated by gravity-flow
201 deposits (e.g. Talling et al., 2012). Deposition from debris flows transitional to high-density, stratified
202 turbulent flows is inferred from the clast supported conglomerate with faintly visible cross-stratification
203 (f2) (e.g. Lowe, 1982; Zavala et al., 2011; Talling et al., 2012). F2 alternates with high-density and low-
204 density turbidity currents, as we infer from the structureless (f3) and or planar laminated or cross-
205 stratified sandstone (f4, f5), respectively. The upward-increasing amalgamation of conglomerate beds
206 represents an increase in energy and is interpreted as mouth bar progradation. Eventually, a decreased
207 depth over the mouth bar causes flow deceleration (Edmonds and Slingerland, 2007), which explains the
208 vertical transition from conglomerate beds into pebbly sandstone that reflect lower energy. Lack of
209 finer-grained facies indicates an absence of interflow beds. The sparse occurrence of *Ophiomorpha*
210 trace fossils supports the interpretation of a marine setting with proximity to the river outlet.

211 FA2.b lacks any marine indicators. However, the interpretation of mouth-bar deposition close the river
212 outlet is supported by the gradual lateral facies change into FA3, local arrangement in dipping
213 accretionary strata, and the lack of erosional channel-shaped surfaces.

214 FA2.a is dominated by gravitational-flow processes, whereas FA2.b by bedload deposition. Despite their
215 different dominant depositional processes, they both represent a closer position relative to the feeding
216 channel than the deposits assigned to FA3–5. This is based on the complete lack of interflow deposits
217 (FA2.a and FA2.b) and low (FA2.a) to absent (FA2.b) bioturbation.

218

219 **FA3 – Mouth bar off-axis**

220 **Description** – FA3 (Fig. 8B) consists of very fine- to fine-grained, 20–50 cm thick sandstone beds that are
221 structureless (f3, Table 1) (Fig. 5C) or show parallel lamination and tabular cross stratification (f4, f5,
222 respectively). Soft-sediment deformation, wood fragments and stringers of extrabasinal clasts (up to 4

223 cm in diameter) are common. The lower part of FA3 displays rare interbedded siltstone to very fine-
224 grained sandstone (f7). Pebbly cross-stratified sandstone (f6, Fig. 5B) dominates the upper part. Sparse
225 and low-diversity bioturbation (BI 0–2, *Ophiomorpha*) characterizes FA3 although rare horizontal
226 bedding planes with BI 4–5 are present. A 20–50 cm thoroughly bioturbated sandstone bed (f9) is
227 commonly found at the base of FA3.

228 FA3 units are 7–8 m thick of which the upper part locally shows arrangement in low-angle dipping
229 accretionary strata (~3° dip towards SSW). FA3 grades laterally into FA2 (mouth bar – axis) or FA4
230 (mouth bar -fringe) and is locally eroded and overlain by FA6 (distributary channel deposits).

231 **Interpretation** – The sedimentary features of FA3 also indicate high energy deposition in a proximal
232 mouth bar setting (e.g. Wright, 1977; Enge et al., 2010; Fidolini and Ghinassi, 2016). This is based on the
233 coarsening-upward nature, the abundance of well-stratified sandstone, the accretionary architecture,
234 and abundant soft sediment deformation. The latter indicates rapid deposition and dewatering by
235 loading, typical for delta front deposition (e.g. Bann et al., 2008). The predominantly absent to sparse
236 bioturbation supports the interpretation of high sedimentation rates and proximity to a river outlet
237 (MacEachern and Bann, 2008). The *Ophiomorpha* structures are typical for high energy settings as well
238 (Pemberton et al., 2001). The rare occurrence of thoroughly bioturbated horizontal bedding reflects
239 short time-windows with reduced depositional energy (MacEachern and Bann, 2008), consistent with an
240 off-axis environment. This indicates sparse interruptions of the otherwise high energy depositional
241 setting and interpreted as the record of interflood periods.

242

243

FA4 – Mouth bar fringe

244 **Description** – A sharp tabular (at outcrop scale) nature characterizes the thin to thick (5–40 cm), very
245 fine- to fine-grained sandstone beds of FA3 (Fig. 5D). They are structureless (f2, Table 1), but show
246 progressively more planar- and tangential cross-stratification (f5) towards the top (Fig. 8C), where
247 trough and cross-stratified pebbly sandstone (f6, Fig. 5B) is locally present. Sandstone beds are in places
248 interbedded with siltstone to very fine-grained sandstone (f3), with common asymmetrical ripples (f8)
249 (Fig. 5E). Mud-drapes are sparse. Stringers of extrabasinal clasts (up to 5 cm diameter) occur locally (Fig.
250 5F). The bioturbation index varies (BI 0–5) and is characterized by a non-uniform but upwards-
251 decreasing trend. We documented high-index bioturbation predominantly on horizontal bedding planes
252 (Fig. 7D) and/or in parallel-laminated siltstones (f7). Trace fossils observed are *Ophiomorpha*,
253 *Thalassinoides*, *Conichnus*, *Palaeophycus*, *Macaronichnus*, *Teichichnus* and *Rosellia* (Fig. 7E). Thoroughly

254 bioturbated sandstone beds (0.3–2 m thick, f9; Fig. 7F) occur locally at the base and / or at the top of
255 FA4.

256 FA4 units are 6–8 m thick and grade laterally into FA3 (mouth bar – off-axis) or FA5 (mouth bar – distal
257 fringe). Fluvial deposits (FA6) incise into FA4 locally (Fig. 9A).

258 **Interpretation** – FA4 represents episodic deposition in a position farther from the river outlet than the
259 previous FA's. This is based on the alternation of upper and lower flow regime bedforms and the non-
260 uniform bioturbation index. The interbedded finer-grained facies were deposited during times of lower
261 energy between river floods (i.e., 'interflood beds' cf. Dalrymple et al., 2015; Gugliotta et al., 2016a),
262 with preservation of a minimal tide-influence. The occurrence of intensely bioturbated horizontal
263 bedding planes and/or interflood beds also suggests longer recurrent times with stable conditions in
264 between deposition of individual sandstone beds (e.g. Gani et al., 2009). The upward-decreasing
265 bioturbation index and local upward-increasing pebble content indicate bar progradation and invreasing
266 proximity to the river mouth (e.g. MacEachern and Bann, 2008; Bhattacharya, 2010).

267

268

FA5 – Mouth bar distal fringe

269 **Description** – FA5 consists of thoroughly bioturbated sandstone beds (1–2 m thick, f9, Table 1) with or
270 without overlying fine-grained sandstone beds with bidirectional cross-stratification (f6). The latter
271 increase upwards in bed thickness from 10 cm to 40 cm, and bidirectionality is supported by
272 paleocurrent measurements (n = 10) (Fig. 8D). These sandstone beds display no mud-draping or trace
273 fossils. FA5 units have thicknesses of 3–4 m and are adjacent to FA4 (mouth bar – fringe).

274 **Interpretation** – FA5 represents mouth bar deposition with decreased river influence compared to FA2–
275 4. The bidirectional cross-stratification indicates that tidal currents were able to fully reverse the river
276 outflow and suggest a strong tide-influence (cf. Martinius and Gowland, 2011).

277

278

FA6 – Fluvial distributary channel

279 **Description** – FA6 consists of fine- to medium-grained sandstone bodies composed of 10–100 cm thick
280 sandstone beds with parallel lamination, tabular (Fig. 6A) and trough cross-stratification (f5, f6, f10,
281 Table 1). Both beds and individual foresets show normal grading and bed thicknesses decrease upwards
282 locally. Erosional flat- and concave-upward surfaces bound the single- and multi-storey sandstone
283 bodies, and in places they are lined with wood debris, muddy rip-up clasts, and/or pebble lag horizons
284 (f11). The single-storey sandstone bodies have average dimensions of ~3/100 m (width/thickness).
285 Multi-storey bodies have erosional bases that form composite surfaces bounding higher-order channel-

286 fill elements with rare lateral accretionary packages. The multi-storey bodies are 250–300 m wide and
287 8–20 m thick, and consist of 2–6 stories (Fig. 9B-C). Internally, individual channel-fill elements average 4
288 m in preserved thickness. Varicolored mottling overprints the uppermost interval of FA6 units in places
289 (Fig. 6B). FA6 is devoid of trace fossils, and only the top surface is commonly bioturbated with *Skolithos*
290 (BI 0–2). Laterally continuous deposits of the Jurassic Morrison Formation also fit with this facies
291 association, but they are outside the focus of this study. FA6 incises into mouth bar deposits (FA2-5) and
292 is also found isolated within interdistributary-bay deposits (FA8).

293 **Interpretation** – FA6 deposition resulted from the migration of two-dimensional and three-dimensional
294 subaqueous bedforms (dune and ripple-scale), and the formation of parallel laminations in upper flow
295 regime conditions, within subaqueous channels (e.g. Flemming, 2000). The absence of bioturbation,
296 marine indicators, and mud-drapes suggests deposition by fully fluvial currents. Preserved fine-grained
297 facies within channel bodies are interpreted as abandoned channel fills, covered by interdistributary fine
298 deposits (FA8). The varicolored mottling indicates weak pedogenesis on previously deposited channel
299 fills and suggests prolonged subaerial exposure. Holbrook (1996) measured average channel depths of
300 10–12 m and widths of 90–180 m for equivalent upstream Mesa Rica trunk channels. This implies that
301 the smaller channel dimensions of FA6 (~3/100 m width/thickness) represent the result of successive
302 downstream bifurcations from the trunk channel. Larger channel dimensions (~250–300/~8 20 m total
303 width/thickness) represent trunk-scale or first-order distributaries. Multi-storey channel deposits relate
304 to repeated occupation of a given location and their deep scouring may indicate a link to forced-
305 regression conditions.

306
307

FA7 – Tide-influenced distributary channel

308 **Description** – FA7 consists of sandstone-dominated heterolithic deposits with predominantly very fine-
309 to fine-grained sharp-based structureless (f3, Table 1) or tabular cross-stratified sandstone beds (f5) that
310 are 10–40 cm thick (Fig. 6C). The cross-stratification is rarely sigmoidal. These sandstone beds alternate
311 with flaser bedding (facies 13; Fig. 6D-E) and/or thin siltstone intervals (1–10 cm thick) (f7, f8). The latter
312 are occasionally mud-draped or double mud-draped and have unidirectional and/or bidirectional ripples
313 in places. Wood debris, mud rip-up clasts, and syneresis cracks are common. Bioturbation occurs both in
314 sandstone and finer-grained siltstone beds, is non-uniform and low (BI 0–3), and includes *Skolithos*,
315 *Macaronichnus*, and *Ophiomorpha*. Erosional concave-upward surfaces bound single-storey (max. 3 m
316 thick, 70 m wide) channel bodies. We documented one multi-storey channel body of 12/75 m
317 (width/thickness).

318 FA7 occurs embedded in fine-grained interdistributary-bay deposits (FA8; Fig. 9D) and incising erosively
319 into mouth-bar deposits (FA2–5). Paleocurrent data (n=42) reveal a mean direction towards NNW.

320 **Interpretation** – FA7 represents the infill of tide-influenced distributary channels. The heterolithic
321 character could result from variations in fluvial discharge (Gugliotta et al., 2016a). However, the
322 occurrence of flaser bedding can be assigned to a tidal origin (Baas et al., 2016), and all channel fills
323 included at least two criteria that may be produced by, although not unique, to tidal processes (e.g.
324 sigmoidal bedding, bidirectional cross-stratification, double mud-draped ripple laminae) (e.g. Nio and
325 Yang, 1991). We therefore interpret a recurrent tide-influence of river currents, rather than a tide-
326 dominance. The bioturbation reflects a low-diversity expression of the *Skolithos* ichnofacies, which
327 supports the interpretation of tidally-affected deposits (Gani et al., 2009). The upstream NNW
328 orientation of the average paleocurrent direction reflects localized tidal flood-dominance.

329

330

FA8 – Interdistributary bay

331 **Description** – FA8 consist predominantly of gray-brown muddy siltstone (f1; Fig. 6F). Very fine- to fine-
332 grained, sharp-based sandstone beds (0.1–0.3 m thick) can be traced for 100–200 m and bed tops
333 commonly exhibit asymmetrical ripples (f8; Fig. 7C). The sandstone beds are generally structureless (f3),
334 occasionally cross-stratified (f5) and interbedded with rippled siltstone (f8). Syneresis cracks common,
335 and bioturbation (BI 0–3) includes *Skolithos*, *Arenicolites*, and *Phycodes*. Isolated sandstone bodies of
336 FA6 (fluvial distributary channel) and FA7 (tide-influenced distributary channel) are found in FA8.

337 **Interpretation** – FA8 represents fine-grained lower-delta-plain to interdistributary-bay deposits, based
338 on its close relation to FA6 and FA7, and absence of coal. The thin-bedded sheet sandstone deposits
339 represent crevasse splays or overbank flow deposits. Trace fossils indicate short-lived marine incursions.
340 The siltstone holds rare dinoflagellates and abundant spores and pollen (Obok-Ikuenobe et al., 2008),
341 which supports the interpretation of brackish conditions.

342

343

FA9 – Estuary

344 **Description** – FA9 consists of fine-grained sandstone beds (0,3–3 m) that fine upward into very fine-
345 grained sandstone beds (5–20 cm) with interbedded siltstone in places. FA9 comprises two subsets;
346 FA9.a is characterized by high index bioturbation (BI 5–6, *Thalassinoides*, *Ophiomorpha*) that obliterates
347 primary structures and bed boundaries. Extrabasinal clasts (diameter < 3 cm) occur dispersed and locally
348 in lag horizons (subangular-subrounded diameter 2–4 cm) together with mud rip-ups (f11, Table 1). The
349 lags are in places overlain by a thin (~5 cm) siltstone package. FA9.b is characterized by sandstone beds

350 (30–60 cm) that are structureless (f3) or reveal parallel lamination, tabular or trough cross-stratification
351 (f5, f6, f9). Composite surfaces bound higher order scour surfaces and are commonly lined with wood
352 debris and muddy rip-up clasts. Bioturbation is absent in the lower part of FA9.a and shows an upward-
353 increasing trend (BI 0–5) in the upper part. Trace fossils include *Thalassinoides*, *Ophiomorpha*, *Planolites*
354 and *Teichichnus*.

355 FA9 has a limited lateral extent of max. 1 km and is found embedded within the underlying fluvial
356 deposits of the Jurassic Morrison Formation; prodelta deposits (FA1) overlie FA9. FA9.a is 2–4 m thick
357 and onlaps the the underlying strata, whereas the basal surface of FA9.b is 6–7 m thick and erosional.

358 **Interpretation** –FA9 represents estuarine deposits, based on localized occurrence, upward-increasing
359 marine influence, and stratigraphic position below prodelta deposits (FA1) (e.g. Holbrook et al., 1987;
360 Van Yperen et al., *in press NMGS*). The high bioturbation index of FA9.a is indicative for conditions
361 favoring trace makers, such as wave-agitation (e.g. MacEachern and Bann, 2008). FA9.b represents the
362 aggradational fluvial infill of existing topographic lows with a progressively increasing marine influence.
363 The stratigraphic position of FA9 relates to the Campana Sandstone Bed (Holbrook et al., 1987).

364

365

Facies distribution

366 Estuarine deposits (FA3) unconformably overlie fluvial strata of the Jurassic Morrison Formation and
367 represent the transgressive infill of topographic lows (Holbrook et al., 1987; Van Yperen et al., *in press*
368 *NMGS*) (Figs 2B, 10). The overlying prodelta (FA1) deposits are present throughout the study area,
369 except in the northwest, and separate Jurassic fluvial strata from Cenomanian Mesa Rica deposits. The
370 latter consist of two sandstone units; Succession 1 (S1) forms a continuous sandstone sheet (6–10 m
371 thick) throughout the study area, whereas Succession 2 (S2) is discontinuous (0–6 m thick) and
372 embedded in interdistributary fines (FA8). S1 and S2 correlate to the lower and upper Mesa Rica,
373 respectively Rica (e.g. Scott et al., 2004; Holbrook et al., 2006) and both successions are capped by a
374 flooding surface with BI 1–5 (*Skolithos*, *Diplocraterion*, *Thalassinoides*) in the study area. These flooding
375 surfaces (Maximum Regressive Surface 1 and 2) represent key stratigraphic surfaces and are used for
376 correlation (Van Yperen et al., *in press NMGS*). They correlate to TS3.1 and TS3.2 (cf. Holbrook et al.,
377 2006; Oboh-Ikuenobe et al., 2008).

378 The sheet-forming S1 contains laterally-extensive mouth bar deposits (FA2–FA5), except in the NW
379 corner of the study area, where fluvial strata (FA6) persist. Previously published work asserted an
380 absence of equivalent shallow marine strata up paleodepositional dip of the study area (e.g. Holbrook et
381 al., 1987; Holbrook and Wright Dunbar, 1992) and drone data collected outside the main study area (Fig.

382 4) and ground truthing confirms this. The S1 is locally incised by composite erosional surfaces containing
383 multi-storey fluvial (FA6) (Fig. 9B, C) and marine-influenced (FA7) channel infill (8–20 thick, 75–300 m
384 wide), and large-scale scours filled with fine-grained material (Fig. 9A). S1 thickens towards the south.
385 The S1 / lower mesa Rica (6–10 m thick) is thin compared to both the upstream fluvial strata (10–15 m,
386 e.g. Holbrook et al., 2006) and downstream fully deltaic strata (12–20 m, Van Yperen et al., *in press JSR*),
387 which reflects deposition at the basin margin (Van Yperen et al., *in press NMGS*).

388 S2 consists of isolated composite fluvial bodies that are amalgamated into multi-lateral single or double
389 stories. They represent mostly fully fluvial channel bodies (FA6), but tide-influenced heterolithic channel
390 bodies occur locally (FA7) (Fig. 9D). The isolated nature of FA6 and FA7 suggests a higher A/S ratio (i.e.,
391 more accommodation or less sediment supply) than during S1 deposition. The S1 and S2 relate to the
392 lower and upper Mesa Rica, respectively (e.g. Holbrook and Wright Dunbar, 1992; Van Yperen et al., *in*
393 *press NMGS*). The overlying strata belong to the paralic Pajarito Formation (e.g. Lucas and Kisucky, 1988;
394 Holbrook and Wright Dunbar, 1992; Holbrook, 1996; Van Yperen et al., *in press NMGS*) and are outside
395 the scope of this paper.

396 Mouth bar (FA2–FA5) paleocurrents reveal a scattered pattern covering 360° variance, which we explain
397 by the intrinsic compensation and growth in radial patterns during mouth bar development. Distributary
398 channel deposits (FA6) show a consistent SSE component whereas the tide-influenced distributary
399 channel deposits have a strong NNW component, supporting the interpretation of bidirectionality (Fig.
400 10).

401

402 MOUTH BAR ARCHITECTURE

403 Components

404 The mouth bar facies associations (FA2-5) represent deposition of sheet-like deposits in a relatively
405 unconfined environment, based on their general lack of deep scours, the laterally extensive individual
406 sandstone beds and the apparent tabular bed geometry. They (FA2-5) form a continuum of deposits that
407 are interpreted as different expressions of deposition close to a river outlet. These sub-environments
408 are referred to as ‘axis’ (FA2), ‘off-axis’ (FA3), ‘fringe’ (FA4) and ‘distal fringe’ (FA5) (Fig. 8), and
409 represent along-strike changes of processes and resulting deposits within a single mouth bar (Fig. 11).
410 This subdivision into mouth bar components is similar to the common classification used to describe
411 deep-water lobe deposits that build basin-floor fan successions (e.g. Hodgson 2009; Prélat et al., 2009;
412 Sychala et al., 2015; Hofstra et al., 2016).

413 Mouth bar facies associations (FA2-5) reveal a predictable trend in flow regime, bed thickness,
414 occurrence of interflood beds, bioturbation index and tide-influence, when moving away from the
415 center to the outer parts of the sedimentary body (Fig. 11). From mouth bar axis to fringe, the
416 occurrence of upper flow regime bedforms and average bed thickness diminishes. Soft-sediment
417 deformation is most common in axis and off-axis deposits (FA2, FA3). The record of interflood beds and
418 bioturbation index progressively increases towards the fringe (FA4; Fig. 11). Interflood beds display
419 varying thicknesses (Fig. 12) and are expressed only by a bioturbated surface in places (Fig. 12A). These
420 thoroughly bioturbated surfaces separate upper flow regime beds and reflect time-windows with
421 reduced depositional energy (MacEachern and Bann, 2008). Therefore, we interpret them as formed
422 during interflood periods, although they likely represent less time than the thicker expressions of
423 interflood beds. In addition, some fringe sections (FA4, FA5) show thoroughly bioturbated top surfaces,
424 which may indicate early abandonment of certain mouth bar components (Fig. 12E, F). The lack of trace
425 fossils in axial deposits can be ascribed to the proximal deltaic setting, in which fresh water dominance
426 overprints the marine influence and makes it unfavorable for infaunal colonization (e.g. MacEachern and
427 Bann, 2008). If no other features indicate a shallow-marine environment, the lateral relationships
428 described are key for an accurate identification of a mouth bar setting.

429

430

Internal geometries and stacking patterns

431 Geometries resulting from the progradation and aggradation of mouth bars during deposition typically
432 reveal a predictable architectural hierarchy with basinward dipping strata at bed scale and lapping
433 relationships at bed and element scale (e.g. Bhattacharya, 2006; Enge et al., 2010; Kurcinka et al., 2018).
434 At bed scale, in the Mesa Rica, subtle lensoid geometries with accompanying onlapping surfaces are
435 sparse in strike-oriented outcrops, which are characterized by a tabular nature and laterally extensive
436 individual sandstone beds. Top truncated terminations of bedding surfaces indicate erosion due to
437 successive bar deposition (Fig. 13). Low-angle accretionary surfaces occur in oblique-oriented sections of
438 axis and off-axis mouth bar deposits (FA2, FA3) (Fig. 14). These oblique- to strike-oriented accretionary
439 surfaces result from mouth bar compensational stacking and growth in radial pattern. Irrespective of
440 their direction, accretionary surfaces are also expected in fringe and distal fringe deposits (FA4, FA5),
441 although axial areas (FA2, FA3) are likely to develop steeper, and more evident foresets (cf. Fidolini and
442 Ghinassi, 2016). The absence of documented accretionary surfaces in fringe sections is ascribed to the
443 low-accommodation setting, which enforces the development of laterally widespread and very low-

444 dipping accretionary surfaces that are difficult to resolve from outcrop data (e.g. Anell et al., 2016; Van
445 Yperen et al., *in press JSR*).

446 At mouth bar scale, bars lap onto older mouth bar strata, creating inter-mouth bar bounding surfaces
447 (Fig. 15). These bounding surfaces are subtle in places and expressed by a sharp contact between two
448 sand beds (Fig. 9, Log 19), or consists of a fine-grained interval mantling the older mouth bar (Fig. 14,
449 Log 3). The latter results from prolonged lowered depositional rates before abandonment. The absence
450 of these fine-grained packages indicates short periods between deposition of successive mouth bars.
451 Additionally, abrupt vertical changes from typical fringe (FA4) to axial (FA2) mouth bar deposits occur in
452 a few places and suggest a spatial shift of active bar deposition as a result of (compensational) stacking
453 of mouth bars. Bar deposits are thicker above thinner units of the underlying mouth bar deposits (e.g.
454 Fig. 12). This is indicative of compensational stacking, and maintenance of a topographic low while the
455 successive mouth was being deposited (cf. Pr elat et al., 2009).

456

457

DISCUSSION

458

Mouth bar dimensions

459 The distance between different mouth bar components observed in the field and their extrapolation
460 provides an estimate of mouth bar dimensions (Fig. 16). In combination with the observed internal
461 geometries and stacking patterns, we utilize this to assess the hierarchy of preserved geometries (Fig. 2);
462 what are the largest elements within the S1 sheet-forming sandstone, mouth bar complexes or delta
463 lobes?

464 The estimation of mouth bar dimensions is challenged by the fragmented outcrop nature and the
465 distribution of data points (Fig. 4; Fig. 16). Log correlation reveals spatial relationships between different
466 mouth bar components, but no complete pinch-out was documented, which limits the assessment of
467 complete mouth bar width. Thus, an overall similar distance between mouth bar components is
468 assumed, which gives a minimum mouth bar width. We exclude the presumable process change
469 towards the distal fringe where sedimentation from suspension fallout would tend to create more
470 laterally extensive plumes.

471 We observe a facies change from fringe to off-axis deposits and back to fringe in ~1.4 km at logs 15, 16,
472 17 (Fowl Canyon; Fig. 9, 16). Axial mouth bar deposits are documented at log 11 (Alamosa) and off-axis
473 and fringe deposits at logs 12, 13 (Dog Canyon; Fig. 16). All these deposits could belong to the same
474 mouth bar, but this causes difficulties to fit the axial mouth bar deposits at log 22 and the fringe
475 deposits inferred from drone data ~900 m south of log 22 (Nana's; Fig. 16). We therefore separate this

476 group of deposits in two mouth bars, of which the one in Dog Canyon has an axis-to-fringe distance of
477 ~900 m, and thus a fringe-axis-fringe minimum width of ~1.8 km. The mouth bar at Alamosa estimates
478 ~1.7 km.

479 The facies architecture and lapping relationships are consistent with components at mouth bar scale
480 rather than depositional trends at lobe scale. We base this on the internal hierarchy, as we rarely
481 observe bounding surfaces and lapping relationships, whilst observations at lobe scale would be
482 expected to reveal numerous bounding surfaces because these result from the amalgamation of mouth
483 bars. In addition, average dimensions of ancient mouth bars range from 1.1 km to 14 km wide with
484 lengths between 2.6 km to 9.6 km (Reynolds, 1999): the inferred dimensions of individual sandstone /
485 mouth bars in the study area (Fig. 16) fit well within this. The S1 sheet-forming mouth bar deposits thus
486 represent amalgamation of mouth bars into a mouth bar complex (Fig. 2).

487

488 **Dominant process regime of the lower Mesa Rica**

489 Mouth bar deposits of the Mesa Rica in the study area represent river-dominated proximal deltaic
490 deposition in a low-accommodation setting. The river-dominance is inferred from the alternation of
491 upper and lower flow regime bedforms, the absent, low-diversity or non-uniform varying bioturbation
492 index, and near-absence of wave-induced bedforms. Based on the latter, the wave-energy was minimal
493 and/or dampened by river discharge.

494 Tidal evidence is absent in mouth bar axis and off-axis deposits (FA2, FA3). Full current-reversals
495 represent unambiguous tidal indicators and are documented as bidirectional cross-stratification at
496 Anna's point and occur in mouth bar distal fringe deposits (FA5) (Fig. 4, Fig. 8D). In most mouth bar
497 fringe deposits (FA4) however, finer-grained interflood beds show mud drapes and rare upstream-
498 migrating current ripples in places. This is inferred as evidence for (moderate) tidal modulation,
499 although the first are not unique tidal indicators. Additionally, tidal action often extends farther
500 landward than marine, salt-water intrusions (Dalrymple et al., 2015). The interflood beds are thoroughly
501 bioturbated and include fully-marine trace fossils. These reflect interflood periods, in which decreased
502 discharge allows the salinity gradient to re-establish in the off axis areas between active mouth bars (e.g.
503 Dalrymple et al., 2015), which in turn influences the ichnological character of the deposit, resulting in
504 more diverse trace-fossil assemblages (Gingras et al., 2002) and/or higher bioturbation indices (e.g.
505 Gugliotta et al., 2016b; Kurcinka et al., 2018). This evidence for salt-water intrusions holds the potential
506 tide influence.

507 Tide energy was variable throughout the study area, based on the differential nature and preservation
508 of tidal indicators. Mouth bar fringes (FA4, FA5) experienced different tidal impact dependent on when
509 and where they formed. For instance, places with weak tidal energy resulted in tidal indicators only
510 present in fine-grained interflood beds, whereas tide-dominated areas favored formation and
511 preservation of sand-prone bidirectional cross-stratified sandstone beds. Both are documented in this
512 study and suggest strike-variability in tidal energy. We reason that decreased river influence allowed
513 localized higher tidal energy. This indicates that the 'background' tidal energy was moderate, but still
514 only recorded in the distal mouth bar fringes, and when river discharge was low.

515

516 **From mouth bar to delta front – controlling factors**

517 The ratio between available accommodation and sediment supply (A/S) is controlled by a combination
518 of allogenic and autogenic factors, but their contribution is often difficult to distinguish because of their
519 close interaction, particularly at high-resolution (e.g. mouth-bar and complex) scales.

520 In this study, at mouth bar scale, deposition occurred within the available accommodation between
521 previously deposited mouth bars (Fig. 15, 16). We link this to autogenic compensation processes and
522 avulsion and/or bifurcation of distributary channels. At the same scale, we infer an overall high
523 sediment supply from the absence of mud and silt in mouth bar axial deposits (FA2), and the rare
524 occurrence of these in mouth bar fringe deposits (FA4, FA5; Fig. 11). Additionally, the absence of trace
525 fossils or low-diversity assemblages (*Ophiomorpha*) in mouth bar axis to off-axis deposits (FA2, FA3) also
526 suggests a rather continuous sedimentation rate, which prohibits colonization by trace makers.
527 *Ophiomorpha* has been related to opportunistic colonization (e.g. Knaust and Bromley, 2012) and has
528 been found in brackish environments and proximal deltaic settings (e.g. MacEachern and Bann, 2008).
529 However, the alternation between upper flow regime bedforms and bioturbated surfaces or interflood
530 beds in fringe deposits (FA4, FA5) result from variations in sediment supply. Variations in sediment
531 supply can be caused by both autogenic and allogenic control and these are often difficult to
532 differentiate. We link the variations to seasonal fluctuations in river discharge and to along-strike
533 differences in sediment distribution within a mouth bar.

534 Amalgamated mouth bar deposits form mouth bar complexes which embody the S1 sheet forming
535 sandstone succession. At this scale, the thinner thickness compared to both the upstream fluvial (e.g.
536 (Holbrook, 2001; Holbrook et al., 2006), and downstream fully deltaic time-equivalent strata (Van
537 Yperen et al., *in press JSR*), reflects deposition close to base level, with vertical limitations on
538 aggradation and incision close to the equilibrium point of the graded stream profile (e.g. Mackin, 1948;

539 Quirk, 1996; Holbrook et al., 2006). This is consistent with the position of the study area at the rim of the
540 Tucumcari Basin, but also with a relatively stable, low-accommodation setting, with either constant sea-
541 level or subjected to slow fluctuations. Limited accommodation promotes faster occupation of all
542 available space in front of the river mouth, and thus accelerates mouth bar depositional cycles (e.g.
543 Olariu and Bhattacharya 2006). The low accommodation also makes lateral sedimentary accretion a
544 prime mechanism for sediment distribution. The lateral shifting locus of mouth bar deposition means
545 that more elapsed time is represented by preserved sediment in three dimensions than in only vertical
546 accumulation (Miall, 2015). Each mouth bar represents a relatively short period of time but the lateral
547 set (mouth bar complex or delta lobe) captures depositional conditions at longer time scales. Successive
548 mouth bar coalescing in such space-limited conditions caused the sheet-like nature (cf. Olariu and
549 Bhattacharya 2006; Van Yperen et al., *in press JSR*).

550 In summary, the stable base level, low-accommodation setting and position of the system in the graded
551 stream profile, are considered the major allogenic controls on the mouth bar complex development. The
552 limited available accommodation led to recurrent avulsion/bifurcation of distributary channels, forcing
553 repetitive and coalescent mouth bar deposition cycles. The resultant compensational stacking and sand-
554 dominated nature of mouth bars reflect the multi-scale interplay of allogenic and autogenic controlling
555 factors.

556

557 **Influence of low accommodation on preservation of interflood beds**

558 Subordinate coastal processes are predominantly recorded in interflood beds. It is important to bear this
559 in mind when interpreting competing coastal processes. If a depositional system or zone only
560 experiences weak tidal energy, the tides modulate, rather than reverse river currents (Martinius and
561 Gowland, 2011; Gugliotta et al., 2016b). In these settings, tidal indicators have highest preservation
562 potential in the interflood beds (e.g. Gugliotta et al., 2016b; Kurcinka et al., 2018).

563 In the study area, the record of interflood beds is subordinate to the record of river flood beds. In
564 general, more time and processes are missing than represented in the rock record (Miall, 2014). River
565 floods have the potential to erode the interflood beds, despite floods only lasting several weeks in
566 medium-sized rivers close to the coast (Dalrymple et al., 2015). If river flood processes are too powerful,
567 interflood deposits are not preserved (cf. Gugliotta et al., 2016a) and the related time is not represented
568 in the rock record. The amount of time contained in these interflood beds is significantly more than in
569 the flood beds (e.g. Miall, 2015).

570 In addition to generalized ideas about preservation potential, the low-accommodation setting limits the
571 preservation potential of interflood deposits in two ways and subsequently masks the true sedimentary
572 processes that were active at time of deposition. First, the low accommodation increases reworking-
573 processes at bed scale and lowers significantly the preservation potential in the axial and off-axis
574 components. The recording of interflood deposits is thus restricted to the mouth bar fringe and distal
575 fringe components (FA4, FA5; Figs 1, 11) because these zones can experience temporary interruptions of
576 the otherwise high energy depositional setting. Second, low accommodation lowers the preservation
577 potential of the fringes themselves. The limited accommodation accelerates mouth bar depositional
578 cycles (e.g. Olariu and Bhattacharya 2006) and increases the reworking potential of older deposits (Van
579 Yperen et al., *in press JSR*). Mouth bar deposition with short recurrence intervals might prevent
580 lithification of previously deposited mouth bar sediment. Additionally, reworking of fringe deposits is
581 expected because their position will likely coincide with the higher energy zones (i.e., axis, off-axis) of
582 successive mouth bars, as they migrate to stack compensationally (Fig. 17). Thus, the low-
583 accommodation setting increases the potential for fringe-reworking which in turn lowers the
584 preservation potential of interflood deposits, as these are predominantly recorded in the fringe and
585 distal fringe mouth bar components. This also explains the sand-prone nature of the fringe and the small
586 differences in overall grain size between mouth bar axis and fringe components. It seems unrealistic to
587 preserve abundant fine-grained fringes in a low-accommodation system like this, but a trend in
588 decreasing energy when moving away from the axis is evident.

589 Lastly, the subordinate record of interflood beds in the study area can be a result of the 'equable'
590 climate of the mid-Cretaceous (Fluteau et al., 2007). Such a warm, low seasonality climate would imply
591 semi-constant high river discharge conditions and could explain the dominance of river flood beds and
592 our interpretation of a rather continuous sedimentation rate with only small variations. However,
593 modeling studies show that there are significant uncertainties in the effect of the sea surface
594 temperature gradient. The latter might cause Hadley cell atmospheric transport reduction which in turn
595 enhances seasonal thermal contrasts (Fluteau et al., 2007; Hasegawa et al., 2012), causing increased
596 variation in river discharge.

597 To summarize, care should be taken when evaluating the relative dominance of process regimes (i.e.,
598 river, tides, waves) in mixed systems. Especially low-accommodation settings are prone to preserve less
599 time and deposits, and in particular the record of interflood periods. These interflood beds are the
600 containers for recording processes captured in finer-grained facies. Their low preservation potential

601 causes potential underestimation of the true influence of these processes in low-accommodation deltaic
602 settings.

603

604 **Implications for other deltaic studies**

605 Our work demonstrates that axis, off-axis, fringe and distal fringe components (FA2–5) can be
606 differentiated in river-dominated mouth bars, even in low-accommodation settings. A growing number
607 of studies document the variability within delta fronts (e.g. Gani and Bhattacharya, 2007; Ainsworth et
608 al., 2016) but few document internal characteristics of mouth bar deposits and their lateral relationships
609 (e.g. Enge et al., 2010; Jerrett et al., 2016; Fidolini and Ghinassi, 2016). Despite the different basinal
610 settings of a shallow lake (Fidolini and Ghinassi 2016) and a foreland basin (Jerrett et al., 2016), both
611 studies reveal similar trends as in the Mesa Rica. Finer-grained facies occur towards the fringe, diversion
612 in paleocurrent directions, and depositional processes change from predominantly high density currents
613 in the axial zone, to an alternation of low and high density deposits in the fringe zones.

614 The Campanian to Maastrichtian Horseshoe Canyon Formation (SW Alberta, Canada) is interpreted as a
615 wave-dominated delta that transitions laterally into fluvial dominated (Ainsworth et al., 2016). The
616 Horseshoe Canyon Formation shows strike-oriented changes in dominant processes at mouth bar
617 complex scale, which allows assessment of the impact of these changes on mouth bar architectures,
618 geometries and facies relationships (Ainsworth et al., 2016). We notice internal variability within
619 individual mouth bars in the strike-oriented correlation panels (Fig. 11 in Ainsworth et al., 2016). The
620 axial components consist of higher energy facies associations (foreshore or upper shoreface) whereas
621 lower shoreface heterolithics become dominant towards the fringes. This demonstrates potential for
622 differentiation of internal mouth bar components in wave-dominated deltas as well as in river-
623 dominated deltas (this study).

624 The recognition of mouth bar components in this study, when compared to previous work, implies that
625 the internal hierarchy of mouth bars is evident and observed regardless of dominant coastal processes
626 and/or depositional setting. Subdivision of mouth bar, mouth bar complexes, and delta lobe deposits
627 into different components can reduce complexity of models deriving from myriad facies subdivisions,
628 and help predicting facies changes and sand distribution.

629

630 **CONCLUSIONS**

- 631 • The Mesa Rica Sandstone represents a river-dominated proximal deltaic succession, based on the
632 recognition of dominant river flood beds, rare tidal-indicators, and a near-absence of wave-induced

633 bedforms. In such a proximal setting, fresh water dominance overprints the marine influence.
634 Lateral relationships are key for accurate identification of depositional sub-environments.

- 635 • Mouth bar deposits of the Mesa Rica Sandstone show four different mouth bar components; axis,
636 off-axis, fringe to distal fringe, in which the occurrence of upper flow regime bedforms and average
637 bed thickness decreases towards the fringe, whilst the record of interflood beds and bioturbation
638 index progressively increases.
- 639 • Subdivision of mouth bars and mouth bar complexes into different components is applicable in
640 other studies, regardless of depositional setting of the studied deltaic succession and/or dominant
641 (deltaic) coastal processes. This improves comparisons between systems and helps predicting facies
642 changes and sand distribution.
- 643 • The low-accommodation setting enforces a negative feedback on the preservation potential of
644 interflood deposits. The recording of these becomes restricted to the fringe and distal fringe mouth
645 bar components due to increased reworking-processes at bed scale and low preservation potential
646 of these beds in the axial and off-axis low-accommodation. The preservation potential of the fringes
647 themselves is in turn lowered because of accelerated mouth bar depositional cycles and consequent
648 increase of fringe-reworking.
- 649 • Care should be taken when evaluating the relative dominance of process regimes (i.e., river, tides,
650 waves) in low-accommodation settings. These are prone to preserve less time and deposits, and in
651 particular interflood beds, yet those are the intervals that predominantly record subordinate coastal
652 processes. Lowered preservation potential leads to underestimation of the true influence of these
653 processes in low-accommodation deltaic settings.
- 654 • Onlapping mouth bar strata and compensational stacking patterns demonstrate the amalgamation
655 of mouth bars into mouth bar complexes. This coalescence of mouth bars resulted in sheet-like
656 geometries. Their sand-rich nature and near-absence of fine-grained interflood deposits reflects
657 deposition in a low A/S setting. Deposition occurred at the rim of the Tucumcari Basin, which caused
658 vertical limitations on aggradation and incision close to the equilibrium point of the graded stream
659 profile.

660

ACKNOWLEDGEMENTS

661 The Lower Cretaceous basinal studies of the Arctic (LoCra) consortium and the Research Centre for
662 Arctic Petroleum Exploration (ARCEX) allocated funding for field expeditions. Sincere thanks go to

663 Stephen Hasiotis for essential feedback on ichnology determination, and Lina Hedvig Line, Cody Myers,
664 Blake Warwick and Edwin Tieman for field-assistance. We thank Gretchen Gurtler and Axel
665 Hungerbuehler from the Mesalands Dinosaur Museum and Natural Sciences Laboratory in Tucumcari for
666 irreplaceable logistical help. Last but definitely not least, we thank the Trigg family for their hospitality
667 and permitting us access to their property, with a special thanks to Sally, Kristen and Rick.

668

669

CONFLICT OF INTEREST

670 There are no conflicts of interest in the preparation or publication of this work.

671

672

DATA AVAILABILITY STATEMENT

673 The data that support the findings of this study are available from the corresponding author upon
674 reasonable request.

675

676

REFERENCES

- 677 Ainsworth, R.B., Vakarelov, B.K., MacEachern, J.A., Nanson, R.A., Lane, T.I., Rarity, F., Dashtgard, S.E. (2016) Process-Driven
678 Architectural Variability In Mouth-Bar Deposits: A Case Study From A Mixed-Process Mouth-Bar Complex, Drumheller,
679 Alberta, Canada. *Journal of Sedimentary Research*, 86, 512–541. <https://doi.org/10.2110/jsr.2016.23>
- 680 Anell, I., Lecomte, I., Braathen, A., Buckley, S.J. (2016) Synthetic seismic illumination of small-scale growth faults, paralic
681 deposits and low-angle clinoforms: A case study of the Triassic successions on Edgeøya, NW Barents Shelf. *Marine and*
682 *Petroleum Geology*, 77, 625–639. <https://doi.org/10.1016/J.MARPETGEO.2016.07.005>
- 683 Baas, J.H., Best, J.L., Peakall, J. (2016) Predicting bedforms and primary current stratification in cohesive mixtures of mud and
684 sand. *Journal of the Geological Society*, 173, 12–45. <https://doi.org/10.1144/jgs2015-024>
- 685 Bann, K.L., Tye, S.C., Maceachern, J.A., Fielding, C.R., Jones, B.G. (2008) Ichnological and sedimentological signatures of mixed
686 wave- and storm-dominated deltaic deposits: examples from the Early Permian Sydney Basin, Australia, in: Hampson, G.J.,
687 Steel, R.J., Burgess, P.M., Dalrymple, R.W. (Eds.), *Recent Advances in Models of Siliciclastic Shallow-Marine Stratigraphy*.
688 SEPM Society for Sedimentary Geology, p. 293. <https://doi.org/https://doi.org/10.2110/pec.08.90.0293>
- 689 Bates, C.C. (1953) Rational theory of delta formation. *American Association of Petroleum Geologists Bulletin*, 37, 2119–2162
- 690 Bhattacharya, J.P. (2006) Deltas, Facies Models Revisited. <https://doi.org/10.2110/pec.06.84.0237>
- 691 Bhattacharya, J.P. (2010) Deltas, in: James, N.P., Dalrymple, R.W. (Eds.), *Facies Models 4*. Geological Association of Canada, pp.
692 233–264
- 693 Broadhead, R.F. (2004) Petroleum geology of the Tucumcari Basin—overview and recent exploratory activity. *New Mexico*
694 *Geology*, 26, 90–94
- 695 Chumakov, N.M., Zharkov, M.A., Herman, A.B., Doludenko, M.P., Kalandadze, N.N., Lebedey, E.L., Rautian, A.S. (1995) Climatic
696 belts of the mid-Cretaceous time. *Stratigraphy and Geological Correlation*, 3, 42–63
- 697 Dalrymple, R.W., Kurcinka, C.E., Jablonski, B.V.J., Ichaso, A.A., Mackay, D.A. (2015) Deciphering the relative importance of fluvial
698 and tidal processes in the fluvial–marine transition, in: Ashworth, P.J., Best, J.L., Parsons, D.R. (Eds.), *Development in*

699 Sedimentology, Fluvial-Tidal Sedimentology. Amsterdam, Elsevier, pp. 3–40. [https://doi.org/10.1016/B978-0-444-63529-](https://doi.org/10.1016/B978-0-444-63529-7.00002-X)
700 7.00002-X

701 DeCelles, P.G. (2004) Late Jurassic to Eocene evolution of the Cordilleran thrust belt and foreland basin system, western U.S.A.
702 *American Journal of Science*, 304, 105–168. <https://doi.org/10.2475/ajs.304.2.105>

703 Dickinson, W.R. (2018) Tectonosedimentary Relations of Pennsylvanian to Jurassic Strata on the Colorado Plateau. Geological
704 Society of America. <https://doi.org/https://doi.org/10.1130/2018.2533>, 2018

705 Edmonds, D.A., Slingerland, R.L. (2007) Mechanics of river mouth bar formation: Implications for the morphodynamics of delta
706 distributary networks. *Journal of Geophysical Research: Earth Surface*, 112, 1–14. <https://doi.org/10.1029/2006JF000574>

707 Elliott, T. (1986) Deltas, in: Reading, H.G. (Ed.), *Sedimentary Environments and Facies*. Blackwell Scientific Publications, Oxford,
708 U.K., pp. 113–154

709 Enge, H. D., Howell, J.A., Buckley, S.J. (2010) The geometry and internal architecture of stream mouth bars in the Panther
710 Tongue and the Ferron Sandstone Members, Utah, U.S.A. *Journal of Sedimentary Research*, 80, 1018–1031.
711 <https://doi.org/10.2110/jsr.2010.088>

712 Enge, Håvard D., Howell, J.A., Buckley, S.J. (2010) Quantifying clinothem geometry in a forced-regressive river-dominated delta,
713 Panther Tongue Member, Utah, USA. *Sedimentology*, 57, 1750–1770. <https://doi.org/10.1111/j.1365-3091.2010.01164.x>

714 Fidolini, F., Ghinassi, M. (2016) Friction- and inertia-dominated effluents in a lacustrine, river-dominated deltaic succession
715 (Pliocene Upper Valdarno Basin, Italy). *Journal of Sedimentary Research*, 86, 1083–1101.
716 <https://doi.org/10.2110/jsr.2016.65>

717 Flemming, B.W. (2000) The role of grain size, water depth and flow velocity as scaling factors controlling the size of subaqueous
718 dunes. *Marine Sandwave Dynamic, International Workshop*, 55–60

719 Fluteau, F., Ramstein, G., Besse, J., Guiraud, R., Masse, J.. (2007) Impacts of palaeogeography and sea level changes on Mid-
720 Cretaceous climate. *Palaeogeography, Palaeoclimatology, Palaeoecology*, 247, 357–381.
721 <https://doi.org/10.1016/J.PALAEO.2006.11.016>

722 Gani, M.R., Bhattacharya, J.P. (2007) Basic Building Blocks and Process Variability of a Cretaceous Delta: Internal Facies
723 Architecture Reveals a More Dynamic Interaction of River, Wave, and Tidal Processes Than Is Indicated by External Shape.
724 *Journal of Sedimentary Research*, 77, 284–302. <https://doi.org/10.2110/jsr.2007.023>

725 Gani, R.M., Bhattacharya, J.P., MacEachern, J.A. (2009) Using ichnology to determine the relative influence of waves, storms,
726 tides, and rivers in deltaic deposits: examples from Cretaceous Western Interior Seaway, USA, in: MacEachern, J.A., Bann,
727 K.L., Gingras, M.K., Pemberton, S.G. (Eds.), *Applied Ichnology: SEPM, Short Course Notes 52*. pp. 200–255

728 Gingras, M.K., Räsänen, M., Ranzi, A. (2002) The significance of bioturbated inclined heterolithic stratification in the southern
729 part of the Miocene Solimoes Formation, Rio Acre, Amazonia Brazil. *Palaios*, 17, 591–601

730 Gugliotta, M., Kurcinka, C.E., Dalrymple, R.W., Flint, S.S., Hodgson, D.M. (2016a) Decoupling seasonal fluctuations in fluvial
731 discharge from the tidal signature in ancient deltaic deposits: an example from the Neuquén Basin, Argentina. *Journal of*
732 *the Geological Society*, 173, 94–107. <https://doi.org/doi:10.1144/jgs2015-030>

733 Gugliotta, Marcello, Flint, S.S., Hodgson, D.M., Veiga, G.D. (2016b) Recognition criteria, characteristics and implications of the
734 fluvial to marine transition zone in ancient deltaic deposits (Lajas Formation, Argentina). *Sedimentology*, 63, 1971–2001.
735 <https://doi.org/10.1111/sed.12291>

736 Hasegawa, H., Tada, R., Jiang, X., Sukanuma, Y., Imsamut, S., Charusiri, P., Ichinnorov, N., Khand, Y. (2012) Drastic shrinking of
737 the Hadley circulation during the mid-Cretaceous Supergreenhouse. *Climate of the Past*, 8, 1323–1337.

738 <https://doi.org/10.5194/cp-8-1323-2012>

739 Hodgson, D.M. (2009) Distribution and origin of hybrid beds in sand-rich submarine fans of the Tanqua depocentre, Karoo Basin,
740 South Africa. *Marine and Petroleum Geology*, 26, 1940–1956. <https://doi.org/10.1016/J.MARPETGEO.2009.02.011>

741 Hofstra, M., Pontén, A.S.M., Peakall, J., Flint, S.S., Nair, K.N., Hodgson, D.M. (2016) The impact of fine-scale reservoir geometries
742 on streamline flow patterns in submarine lobe deposits using outcrop analogues from the Karoo Basin. *Petroleum*
743 *Geoscience*, 23, 159–176. <https://doi.org/10.1144/petgeo2016-087>

744 Holbrook, J.M. (1996) Complex fluvial response to low gradients at maximum regression; a genetic link between smooth
745 sequence-boundary morphology and architecture of overlying sheet sandstone. *Journal of Sedimentary Research*, 66,
746 713–722. <https://doi.org/10.1306/D42683EC-2B26-11D7-8648000102C1865D>

747 Holbrook, J.M. (2001) Origin, genetic interrelationships, and stratigraphy over the continuum of fluvial channel-form bounding
748 surfaces: An illustration from middle Cretaceous strata, Southeastern Colorado. *Sedimentary Geology*, 144, 179–222.
749 [https://doi.org/10.1016/S0037-0738\(01\)00118-X](https://doi.org/10.1016/S0037-0738(01)00118-X)

750 Holbrook, J.M., Scott, R.W., Oboh-Ikuenobe, F.E. (2006) Base-level buffers and buttresses: a model for upstream versus
751 downstream control on fluvial geometry and architecture within sequences. *Journal of Sedimentary Research*, 76, 162–
752 174. <https://doi.org/10.2110/jsr.2005.10>

753 Holbrook, J.M., White, D.C. (1998) Evidence for subtle uplift from lithofacies distribution and sequence architecture: Examples
754 from lower Cretaceous strata of northeastern New Mexico, in: Shanley, K.W., McCabe, P.J. (Eds.), *Relative Role of Eustasy,*
755 *Climate, and Tectonism in Continental Rocks*. SEPM Special Publication, pp. 123–132

756 Holbrook, J.M., Wright Dunbar, R. (1992) Depositional history of Lower Cretaceous strata in northeastern New Mexico :
757 Implications for regional tectonics and depositional sequences. *Geological Society Of America Bulletin*, 104, 802–813.
758 [https://doi.org/10.1130/0016-7606\(1992\)104<0802](https://doi.org/10.1130/0016-7606(1992)104<0802)

759 Holbrook, J.M., Wright, R., Kietzke, K.K. (1987) Stratigraphic relationships at the Jurassic-Cretaceous boundary in east-central
760 New Mexico, in: Lucas, S.G., Hunt, A.P. (Eds.), *New Mexico Geological Society, 38th Annual Fall Field Conference*
761 *Guidebook*. pp. 161–165

762 Jerrett, R.M., Bennie, L.I., Flint, S.S., Greb, S.F. (2016) Extrinsic and intrinsic controls on mouth bar and mouth bar complex
763 architecture: Examples from the Pennsylvanian (Upper Carboniferous) of the central Appalachian Basin, Kentucky, USA.
764 *Bulletin of the Geological Society of America*, 128, 1696–1716. <https://doi.org/10.1130/B31429.1>

765 Kisucky, M.J. (1987) Sedimentology, stratigraphy and paleogeography of the lower Cretaceous Mesa Rica delta system,
766 Tucumcari Basin, east-central New Mexico. Albuquerque, University of New Mexico

767 Knaust, D., Bromley, R.G. (2012) Trace fossils as indicators of sedimentary environments, *Developmen.* ed. Elsevier Science

768 Kues, B.S. (1997) New Bivalve Taxa from the Tucumcari Formation (Cretaceous , Albian), New Mexico , and the Biostratigraphic
769 Significance of the Basal Tucumcari Fauna Author (s): Barry S . Kues Published by : Paleontological Society Stable URL :
770 [https://doi.org/10.1016/S0016-7606\(1997\)104<0802](https://doi.org/10.1016/S0016-7606(1997)104<0802)
Journal of Paleontology, 71, 820–839

771 Kurcinka, C., Dalrymple, R.W., Gugliotta, M. (2018) Facies and architecture of river-dominated to tide-influenced mouth bars in
772 the lower Lajas Formation (Jurassic), Argentina. *AAPG Bulletin*, 102, 885–912.
773 <https://doi.org/10.1306/0609171618917155>

774 Lowe, D.R. (1982) Sediment gravity flows: II. Depositional models with special reference to the deposits of high-density turbidity
775 currents. *Journal of Sedimentary Petrology*, 52, 279–297

776 Lucas, S., Kisucky, M.J. (1988) Type and reference sections of the Tucumcari, Mesa Rica and Pajarito Formations of east-central

777 New Mexico. *New Mexico Geology*, 10, 82–89

778 MacEachern, J.A., Bann, K.L. (2008) The Role of Ichnology in Refining Shallow Marine Facies Models, in: Hampson, G.J., Steel,
779 R.J., Burgess, P.M., Dalrymple, R.W. (Eds.), *Recent Advances in Models of Siliciclastic Shallow-Marine Stratigraphy*. SEPM,
780 pp. 73–116. <https://doi.org/doi:10.2110/pec.08.90.0073>

781 MacKenzie, D.B., Poole, D.M. (1962) Provenance of Dakota Group Sandstones of the Western Interior. Wyoming Geological
782 Association

783 Mackin, J.H. (1948) Concept of the graded river. *Geological Society of America Bulletin*, 59, 463–512

784 Martinus, A.W., Gowland, S. (2011) Tide-influenced fluvial bedforms and tidal bore deposits (Late Jurassic Lourinhã Formation,
785 Lusitanian Basin, Western Portugal). *Sedimentology*, 58, 285–324. <https://doi.org/10.1111/j.1365-3091.2010.01185.x>

786 Miall, A.D. (2014) The emptiness of the stratigraphic record: a preliminary evaluation of missing time in the Mesaverde Group,
787 Book Cliffs, Utah, U.S.A. *Journal of Sedimentary Research*, 84, 457–469.
788 <https://doi.org/https://doi.org/10.2110/jsr.2014.40>

789 Miall, A.D. (2015) Updating uniformitarianism: stratigraphy as just a set of “frozen accidents.” *Geological Society, London,*
790 *Special Publications*, 404, 11–36

791 Mulder, T., Syvitski, J.P.M., Migeon, S., Faugères, J.C., Savoye, B. (2003) Marine hyperpycnal flows: Initiation, behavior and
792 related deposits. A review. *Marine and Petroleum Geology*, 20, 861–882.
793 <https://doi.org/10.1016/j.marpetgeo.2003.01.003>

794 Nio, S.-D., Yang, C.-S. (1991) Diagnostic attributes of clastic tidal deposits: a review, in: Smith, D., Reinson, G.G.E., Zaitlin, B.A.,
795 Rahmani, R.A. (Eds.), . CSPG Special Publications, pp. 3–27

796 Oboh-Ikuenobe, F.E., Holbrook, J.M., Scott, R.W., Akins, S.L., Evetts, M.J., Benson, D.G., Pratt, L.M. (2008) Anatomy of
797 epicontinental flooding: Late Albian-Early Cenomanian of the southern U.S. Western Interior Basin, in: Pratt, B.R.,
798 Holmden, C. (Eds.), *Dynamics of Epeiric Seas*. Geological Association of Canada, Special Paper, pp. 201–227.
799 [https://doi.org/10.1016/0016-7037\(86\)90064-5](https://doi.org/10.1016/0016-7037(86)90064-5)

800 Olariu, C., Bhattacharya, J.P. (2006) Terminal distributary channels and delta front architecture of river-dominated delta
801 systems. *Journal of Sedimentary Research*, 76, 212–233. <https://doi.org/10.2110/jsr.2006.026>

802 Pemberton, S.G., Spila, M.V., Pulham, A.J., Saunders, T., MacEachern, J.A., Robbins, D., Sinclair, I. (2001) Ichnology and
803 sedimentology of shallow and marginal marine systems: Ben Nevis and Avalon Reservoirs, Jeanne D’Arc Basin. *Geological*
804 *Association of Canada, Short Course Notes*, 15, 353

805 Postma, G. (1990) Depositional architecture and facies of river and fan deltas: a synthesis, in: Colella, A., Prior, D.B. (Eds.),
806 *Coarse-Grained Deltas*. International Association of Sedimentologists, Special Publication, pp. 13–27

807 Prêlat, A., Hodgson, D.M., Flint, S.S. (2009) Evolution, architecture and hierarchy of distributary deep-water deposits: a high-
808 resolution outcrop investigation from the Permian Karoo Basin, South Africa. *Sedimentology*, 56, 2132–2154.
809 <https://doi.org/10.1111/j.1365-3091.2009.01073.x>

810 Quirk, D.G. (1996) ‘Base profile’: a unifying concept in alluvial sequence stratigraphy. *Geological Society, London, Special*
811 *Publications*, 104, 37–49. <https://doi.org/10.1144/GSL.SP.1996.104.01.04>

812 Reynolds, A.D. (1999) Dimensions of paralic sandstone bodies. *American Association of Petroleum Geologists Bulletin*, 83, 211–
813 229

814 Scott, R.W. (1974) Bay and shoreface benthic communities in the Lower Cretaceous. *Lethaia*, 7, 315–330.
815 <https://doi.org/10.1111/j.1502-3931.1974.tb00907.x>

816 Scott, R.W., Holbrook, J.M., Oboh-Ikuenobe, F.E., Evetts, M.J., Benson, D.G., Kues, B.S. (2004) Middle Cretaceous stratigraphy,
817 southern western interior seaway, New Mexico and Oklahoma. *Rocky Mountain Association of Geologists*, 41, 33–61

818 Scott, R.W., Oboh-ikuenobe, F.E., Benson, D.G., Holbrook, J.M. (2009) Numerical age calibration of the Albian/Cenomanian
819 boundary. *Stratigraphy*, 6, 17–32

820 Scott, R.W., Oboh-Ikuenobe, F.E., Benson, D.G., Holbrook, J.M., Alnahwi, A. (2018) Cenomanian-Turonian flooding cycles: U.S.
821 Gulf Coast and Western Interior. *Cretaceous Research*, 89, 191–210. <https://doi.org/10.1016/J.CRETRES.2018.03.027>

822 Spychala, Y.T., Hodgson, D.M., Prélat, A., Kane, I.A., Flint, S.S., Mountney, N.P. (2017) Frontal and Lateral Submarine Lobe
823 Fringes: Comparing Sedimentary Facies, Architecture and Flow Processes. *Journal of Sedimentary Research*, 87, 75–96.
824 <https://doi.org/10.2110/jsr.2017.2>

825 Talling, P.J., Masson, D.G., Sumner, E.J., Malgestini, G. (2012) Subaqueous sediment density flows: Depositional processes and
826 deposit types. *Sedimentology*, 59, 1937–2003. <https://doi.org/10.1111/j.1365-3091.2012.01353.x>

827 Taylor, A.M., Goldring, R. (1993) Description and analysis of bioturbation and ichnofabric. *Journal of the Geological Society*, 150,
828 141–148. <https://doi.org/10.1144/gsjgs.150.1.0141>

829 Waage, K.M. (1955) Dakota Group in northern Front Range foothills, Colorado. *U.S. Geological Survey Professional Paper*, 274-B,
830 B15–B51

831 Wellner, R., Beaubouef, R., Van Wagoner, J., Roberts, H., Sun, T. (2005) Jet-plume depositional bodies - The primary building
832 blocks of the Wax Lake Delta. *Gulf Coast Association of Geological Societies, Transactions*, 55, 867–909

833 Wright, L.D. (1977) Sediment transport and deposition at river mouths: A synthesis. *Geological Society of America Bulletin*, 88,
834 857–868

835 Wright, L.D., Coleman, J.M. (1973) Variations in morphology of major river deltas as functions of ocean wave and river
836 discharge regimes, American Association of Petroleum Geologists Bulletin. American Association of Petroleum Geologists.
837 <https://doi.org/10.1306/819A4274-16C5-11D7-8645000102C1865D>

838 Zavala, C., Arcuri, M., Di Meglio, M., Diaz, H.G., Contreras, C. (2011) A genetic facies tract for the analysis of sustained
839 hyperpycnal flow deposits, in: Slatt, R.M., Zavala, C. (Eds.), *Sediment Transfer from Shelf to Deep Water—Revisiting the*
840 *Delivery System*. AAPG Studies in Geology, pp. 31–52. <https://doi.org/10.1306/13271349St613438>

841 Van Yperen, A.E., Holbrook, J.M., Poyatos-Moré, M., Midtkandal, I., in press, Coalesced delta front sheet-like sandstone bodies
842 from highly avulsive distributary channels: the low-accommodation Mesa Rica Sandstone (Dakota Group, New Mexico,
843 USA), *Journal of Sedimentary Research*

844 Van Yperen, A.E., Line, L.H., Holbrook, J.M., Poyatos-Moré, M., Midtkandal, I., in press, Revised stratigraphic relationships of the
845 Dakota Group in the Tukumcari Basin (San Miguel county, New Mexico, USA), 70th ed. *New Mexico Geological Society*
846 *Guidebook*

Summary of facies (f) in the studied interval at the Trigg Ranch study area, east-central New Mexico

Description	Grainsize	Structures	Biogenic structures	Interpretation
f1 Muddy siltstone	Mud - Si	Structureless, gray or gray-brown muddy siltstone. In places fissile. Max 5 m thick. Commonly vegetated.	BI 4-6: <i>Phycosiphon</i> , <i>Thalassionoides</i> , <i>Planolites</i> , <i>Teichichnus</i> , <i>Chondrites</i> , <i>Helminthopsis</i> . Locally, no bioturbation observed.	Suspension fallout, low sedimentation rates in an open marine setting (bioturbated), or brackish setting (non-bioturbated).
f2 Conglomerate	Cgl	Sharp-based, clast-supported, conglomerate, often crudely stratified. No or normal grading. Sub-angular to sub-rounded, poorly - moderately sorted extrabasinal and intrabasinal clasts, average ϕ 0,5-2 cm (max ϕ 6 cm). Extrabasinal clasts are predominantly quartz and chert. Fine- to medium-grained matrix. Bed thickness 10-30 cm.	BI 0-2: <i>Ophiomorpha</i>	Predominantly deposition from high-density turbidity currents. When grading and stratification is absent; deposition from debris flows transitional to high-density turbulent flow.
f3 Structureless sandstone	VF - F	Erosional, sharp-based, structureless sandstone with normal grading. Bed tops exhibit asymmetrical ripples locally. Bed thickness 5-80 cm.	BI 0-5: <i>Ophiomorpha</i> , <i>Skolithos</i> , <i>Thalassionoides</i> , <i>Conichnus</i> , <i>Palaeophycus</i> , <i>Rosellia</i> . High BI-indices on horizontal bedding planes.	Lack of structure might be due to intensive surface weathering. Rapid suspension fall out. Waning flow energy when rippled top surface.
f4 Parallel-laminated sandstone	VF - F	White and brown sharp-based and -topped, parallel-laminated sandstone. Bed tops exhibit asymmetrical ripples locally. Bed thickness 20-70 cm.	BI 0-3: <i>Skolithos</i> , <i>Ophiomorpha</i> , <i>Rosellia</i>	Upper flow conditions
f5 Tabular cross-stratified sandstone	VF - M	Sharp-based and -topped, local lower erosive base, planar and tangential tabular cross-stratified sandstone. Locally, bidirectional. Bed thickness 20-50 cm. In places organized in low-angle accretionary packages. Local wood-remains.	BI 0-4: <i>Ophiomorpha</i> , <i>Skolithos</i> , <i>Thalassionoides</i> , <i>Conichnus</i> , <i>Palaeophycus</i> , <i>Rosellia</i> . High BI-indices on horizontal bedding planes.	Migrating straight-crested or sinuous dunes with and without flow superation, lower flow regime.
f6 Pebbly sandstone	F - F-M	Pebbly sandstone with trough and tangential cross-stratification. Intra- and extrabasinal pebbels, average ϕ 0,5-1 cm (max ϕ 3 cm). In places organized in low-angle accretionary packages.	Not observed	High-energy unidirectional traction currents and bed load deposition.
f7 Parallel-laminated siltstone	Si - VF	Parallel-laminated siltstone, in places mud-draped. 1-20 cm thick.	Not observed	Gentle flow activity with potential tide-influence.
f8 Asymmetrical ripple-laminated siltstone to sandstone	VF - F	Unidirectional current ripples in sharp-based sandstone beds. Sparse climbing and/or sigmoidal ripples. Bed thickness 3-40 cm.	BI 0-3: <i>Skolithos</i> , <i>Ophiomorpha</i> , <i>Macharonichnus</i>	Migrating straight-crested ripples. Lower flow regime. Climbing ripples indicate high rates of deposition.
f9 Thoroughly bioturbated sandstone	Si - F	Sharp-based and -topped sandstone beds. Bioturbation obliterates original sedimentary features and bed boundaries. 20 cm-3 m thick.	BI 5-6: <i>Thalassionoides</i> , <i>Ophiomorpha</i>	Bioturbation favourable conditions (optimized oxygen, salinity, temperature).
f10 Trough cross-stratified sandstone	F - M	Single to several sets of trough cross-bedding. Set thickness 15-110 cm.	Not observed	Migrating sinuous or linguoid dunes. Lower flow regime.
f11 Pebble lag	Cgl	Erosional basal surface with extrabasinal clasts in a finer sandstone matrix. Clast- or matrix-supported, subangular to subrounded. Includes mud-silt rip-up clasts and/or wood debris locally.	Not observed	High-energy fluvial channel base. When situated at the base of facies structureless or muddy siltstone, potential lag formed by wave-erosion and reworking.
f12 Paleosol	Si - Vf	Purple siltstone with gray rhizoliths and yellow mottling. Yellow-grey siltstone with yellow mottling. Locally, soil development overprints parallel-laminated sandstone.	Mottling, rhizoliths	Subaerial exposure, post-deposition weak to moderate pedogenic development.
f13 Flaser bedding	VS-F	Ripple- and dune-scale cross-stratified sandstone with single or double mud drapes. Locally, climbing ripples and / or bidirectional ripples.	BI 0-1: <i>unidentified</i>	Current reversals in subtidal zone. Climbing ripples indicate high rates of deposition.

848

849

FIGURE CAPTIONS

850 FIGURE 1 Schematic depiction of facies stacking patterns with seasonal bedding (i.e., river flood and
851 interflood beds). River flood beds are thicker and more amalgamated towards the top and in the
852 proximal part of the mouth bar. A progressive decrease of preserved interbedding shows a similar trend.
853 Note that the occurrence of interflood beds is expected to be lower in the scenario with a lower A/S
854 ratio. Modified after Gugliotta et al. (2016a).

855

856 FIGURE 2 Coalescence of individual mouth bars forms mouth bar complexes and delta lobes, which
857 together form the building blocks of a delta system. Mouth bar complexes are related to the same pulse
858 of progradation and their shallow distributary channel network are genetically linked. Mouth bar lobes
859 consist of mouth bar complexes related to the same primary distributary feeder channel. Note that the
860 occurrence of fringe deposits is limited in proximal areas at all scales. Terminology used in previous
861 works and cited in the text is listed.

862

863 FIGURE 3 (A) Regional map of the Western Interior during the Early – Late Cretaceous (Albian-
864 Cenomanian) showing the approximate location of the Western Interior Seaway extent (light blue,
865 Blakey, 2014) and main basins that formed during Laramide Orogeny and Colorado Orogeny (modified
866 after Van Yperen et al. *in press-JSR*). The study area is situated at the rim of the Tucumcari Basin (red
867 square). GRB = Green River Basin; UB= Uinta Basin; DB (Colorado) = Denver Basin; SJB = San Juan Basin,
868 TB = Tucumcari Basin; DB (New Mexico) = Dalhart Basin; BD = Bravo Dome. (B) Chronostratigraphic chart
869 for the Jurassic to Cenomanian successions in Northeastern (NE) and East-central New Mexico.
870 References used for compilation; Waage, 1955; Holbrook et al., 2006; Oboh-Ikuenobe et al., 2008; Van
871 Yperen et al., *JSR*; Van Yperen et al., *NMGS*. Albian-Cenomanian boundary from Scott et al. (2018). SB =
872 Sequence boundary, TS = Transgressive Surface

873

874 FIGURE 4 Geologic map of the study area around the Trigg Ranch, in San Miguel County, showing the
875 outcrop extent and location of the collected dataset. Drone data was collected outside the main study
876 area as well (see inset). Locations of the photopanoramas in Fig. 13, 14 and 15 are also indicated.

877

878 FIGURE 5 Photographs of selected facies (Table 1). (A) Clast supported conglomerate (f2) alternating
879 with structureless sandstone (f3) and/or planar lamination (f4) or cross-stratification (f5). The contact

880 represents an erosive surface related to the reworking of successive bypassing events. This facies
881 assemblage occurs in axial mouth-bar deposits (FA2). (B) Trough cross-stratified pebbly sandstone (f6) in
882 axial mouth-bar deposits (FA2). Common in off-axis deposits (FA3) as well. (C) Structureless sandstone
883 (f3) with wood fragments and low index bioturbation (BI 1) in mouth-bar off-axis deposits (FA3).
884 Common in mouth-bar fringe deposits (FA4) as well. O = *Ophiomorpha*. (D) Thin to thick-bedded (5–40
885 cm), fine-grained structureless sandstone (f3) and cross-stratified sandstone (f5) in mouth bar fringe
886 (FA4) deposits. Interbedding with asymmetrical ripple-laminated sandstone (facies 8). (E) Structureless
887 sandstone (f3) interbedded with asymmetrical ripple-laminated sandstone (f8), with high-index
888 bioturbation on horizontal bedding planes. This is typical for mouth bar fringe deposits (FA4). (F)
889 Bioturbated parallel laminated sandstone (f4) with scattered pebble lags in mouth bar fringe deposits
890 (FA4). O = *Ophiomorpha*. 15-cm pencil and 33-cm hammer for scale.

891
892 FIGURE 6 Photographs of selected facies (Table 1). (A) Bedsets of tabular cross-stratified sandstone (f5)
893 in fluvial distributary channel-fill deposits (FA6). (B) Weak pedogenesis overprinting parallel-laminated
894 sandstone (f6) at the top of a fluvial distributary channel fill (FA6). (C) Tide-influenced distributary
895 channel-fill deposits (FA7), with bidirectional tabular cross-stratified sandstone (f5) and ripple-laminated
896 sandstone (f8), overlying sand-dominated heterolithic deposits (f3, f13). (D) Flaser bedding (f13) with
897 climbing ripples and upwards-increasing sand content, in tide-influenced distributary channel-fill
898 deposits (FA7). (E) Zoom-in of c, with detail of flaser bedding (f13). (F) Gray-brown muddy siltstone (f1),
899 interpreted as part of interdistributary bay deposits (FA8). 15-cm pencil and 33-cm hammer for scale.

900
901 FIGURE 7 Photographs of selected ichnotaxa. (A) Muddy siltstone with BI 4–5 in prodelta deposits (FA1).
902 (B) Alternating conglomerate (f2) and structureless sandstone (f3) with non-uniform BI 0–3 in axial
903 mouth-bar deposits (FA2). (C) Structureless sandstone beds with bed tops that exhibit asymmetrical
904 ripples (f3) interbedded with silt to very-fine-grained sandstone (f7). Trace fossils include *Skolithos* and
905 several undefined traces. This facies and trace fossil assemblage occur in interdistributary bay deposits
906 (FA8). (D) High-index (BI 4–5) bioturbation at a basal bedding plane in mouth-bar fringe deposits (FA4).
907 (E) Low-diversity trace fossil suite in mouth bar off-axis to fringe deposits (FA3, FA4). (F) Thoroughly
908 bioturbated sandstone (BI 5–6) in which traces are only sporadically identifiable. (G) Bioturbated top
909 surface in mouth-bar off-axis deposits (FA3). Th = *Thalassinoides*, He = *Helminthopsis*, Pl = *Planolites*, S =
910 *Skolithos*, O = *Ophiomorpha*, Pa = *Palaeophycus*, C = *Conichnus*, R = *Rosselia*. 15-cm pencil and 33-cm
911 hammer for scale.

912

913 FIGURE 8 Mouth bar facies associations (FA2-FA5) in the low-accommodation Mesa Rica deltaic system.
914 Selected photographs show representative parts or complete logged sections of the different sub-
915 environments referred to as 'axis' (FA2), 'off-axis' (FA3), 'fringe' (FA4), and 'distal fringe' (FA5).
916 Bidirectional paleocurrent measurements support the interpretation of tide-influenced distal fringe
917 deposits (D).

918

919 FIGURE 9 Photographs of fluvial facies associations that occur in the S1 and S2 successions. (A) Fine-
920 grained abandoned channel fill incising S1 mouth bar deposits. Location: Rain Ridge (Fig.4). (B)
921 Multistory fluvial distributary channel (FA6) bound by composite erosional surface, within the S1.
922 Location: Anna's point (Fig. 4). (C) Interpretation and line drawing of b. The multistory fluvial body
923 incises into the underlying Jurassic Morrison Formation. (D) Heterolithic deposits interpreted as tide-
924 influenced distributary channel fill (FA7), in S2. Location: Fowl Canyon (Fig. 4)

925

926 FIGURE 10. Correlation fence diagram illustrating 3D facies distribution offered by physical correlation
927 and interpolation of strike-oriented cross sections. Map shows the true orientation and distances,
928 whereas the diagram is simplified to maximize clarity. Today's topography is visualized, except for the
929 S1 succession because this is the main focus of the paper. The MRS2 is used as a datum for the fence
930 diagram. Sketch logs are not depicted and rose diagrams display paleocurrent data from S1 grouped
931 according to facies associations. MRS = Maximum Regressive Surface.

932

933 FIGURE 11 Schematic representation of a strike-oriented cross-section through an individual mouth bar
934 indicating the distinguished components. Displayed logs are taken from originally measured logs to
935 enhance differences between components. Mouth bar axis to distal fringe trends reveal changes in flow
936 regime, bed thickness, occurrence of interflood beds, bioturbation index, and tide-influence. Not all
937 fringe components show tide-influence. An increase in tide-influence (imaged by bidirectional cross-
938 stratification, right limb of the mouth bar) is accompanied with a decreasing bioturbation index. See text
939 for further discussion.

940

941 FIGURE 12 River flood and interflood beds in FA4 deposits (mouth-bar fringe). River flood beds have a
942 sharp base, coarser grain size and lower bioturbation index (BI 0-3) than interflood deposits. In places,
943 the interflood is represented only by a thoroughly bioturbated surface (a). Bioturbated horizons

944 commonly require several months to form (e.g. Gringras et al., 2002) and contrast with upper flow
945 regime beds interpreted as river flood event beds, which can be as short as a few hours (Gugliotta et al.,
946 2016a and references herein). Note that the upper part of the facies association is thoroughly
947 bioturbated in e, f which indicates early abandonment. Th = *Thalassinoides*, R = *Rosselia*. 15-cm pencil
948 for scale.

949
950 FIGURE 13 (a) Field photograph showing along-strike internal mouth bar geometries. The white arrow
951 indicates average palaeocurrent direction. Inset box shows location of b. (b) Zoom in on subtle lensoid
952 geometries. (c) Subtle lensoid geometries show accompanying onlapping, downlapping, and truncation
953 relationships.

954
955 FIGURE 14 Field photograph (and interpretation) of a mouth bar section, showing low-angle
956 accretionary surfaces (clinoforms) top-truncated by distributary channels. Note the cross-stratification
957 that is locally in opposite direction than larger accretionary surfaces. Clinoforms could evidence oblique
958 compensational growth of mouth bars as these are complex geobodies that grow in a radial pattern. See
959 Figs 4, 10 for location. See text for further discussion.

960
961 FIGURE 15 (A) Strike-oriented photograph, see Figs 4, 10 for location. (B) Line drawing and
962 interpretation of A, showing onlapping relationships between bed sets. (C) Vertical exaggeration of B,
963 enhancing onlapping relationships (red arrow). The mouth bar laps onto older fringe strata, creating
964 inter-mouth bar bounding surfaces. This represents the bounding surface between two individual mouth
965 bars in which the younger mouth bar onlaps the off-axis and fringe sections of the previous. Note that
966 the older mouth bar shows lateral facies transitions from heterolithic fringe (D), to sand-prone off-axis
967 deposits (E), to mouth bar axis deposits with common soft sediment deformation and an absence of
968 trace fossils (F).

969
970 FIGURE 16 (A) Mouth bars range 1.4–1.8 km, based on the distribution of mouth bar components,
971 distributary channels and interpolation between them. Where no mouth bar abbreviation is indicated,
972 strata are eroded by trunk channels. These trunk channels are not visualized in the figure as these
973 reflect a later generation and feed a delta outside and down-dip of the study area. Paleocurrent
974 readings were collected from mouth bar deposits. (B) Schematic representation of the relationship

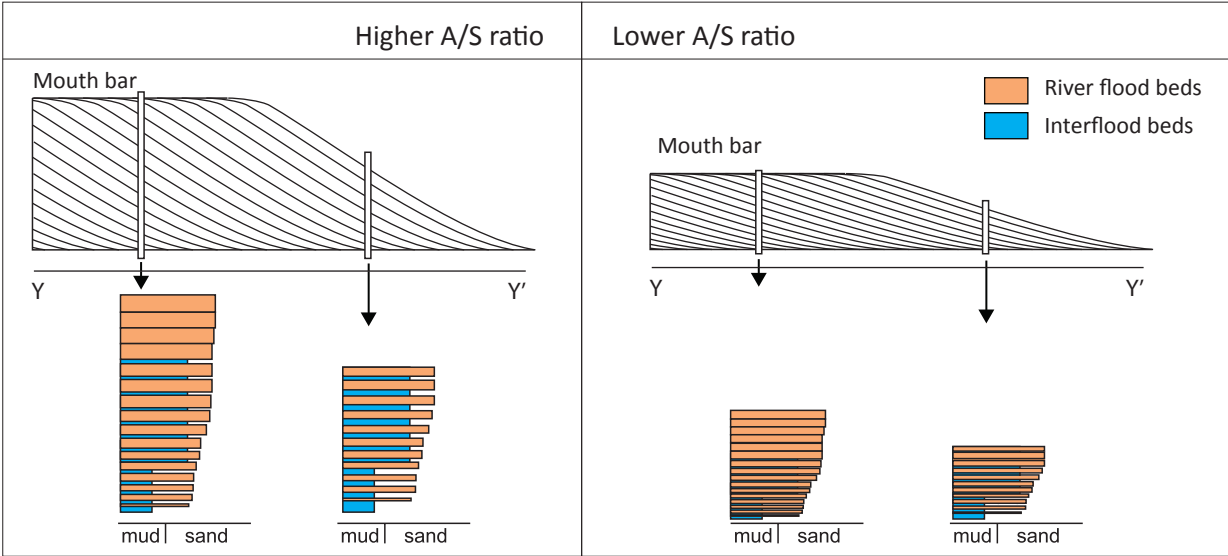
975 between two individual mouth bars. This is based on observed abrupt vertical changes, which we
976 interpreted as a spatial shift and stacking of individual mouth bars.

977

978

979 FIGURE 17: From individual mouth bar to mouth bar complex. (A) A single mouth bar shows decreasing
980 river jet strength and increase in recording of interflood beds from axis to distal fringe. (B) Multiple
981 mouth bars occupy all available accommodation. Every stage (t1-t4) shows the cumulative preservation
982 of river jet deposits and interflood beds. Successive deposition of mouth bars causes reworking of
983 fringes and subsequently erodes the previously deposited interflood beds, thereby the potential
984 recording of subordinate coastal processes. (C) Eventually, a primary distributary channel erodes
985 through the mouth bar complex and will initiate new mouth bar deposition beyond the stranded mouth
986 bar complex.

987



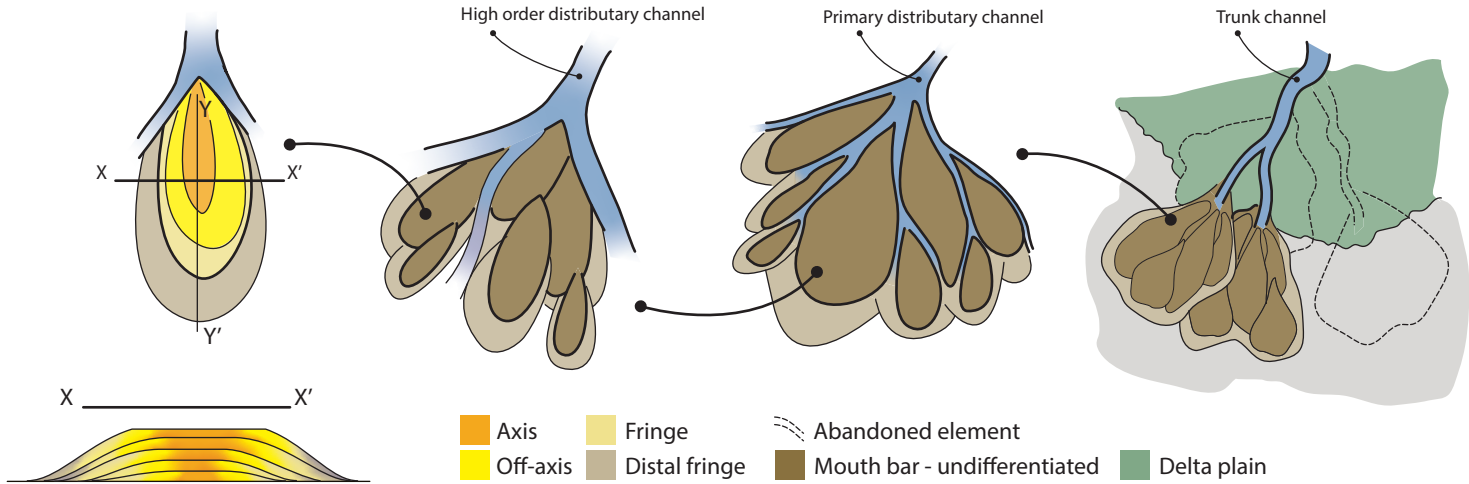
This study:

Mouth bar

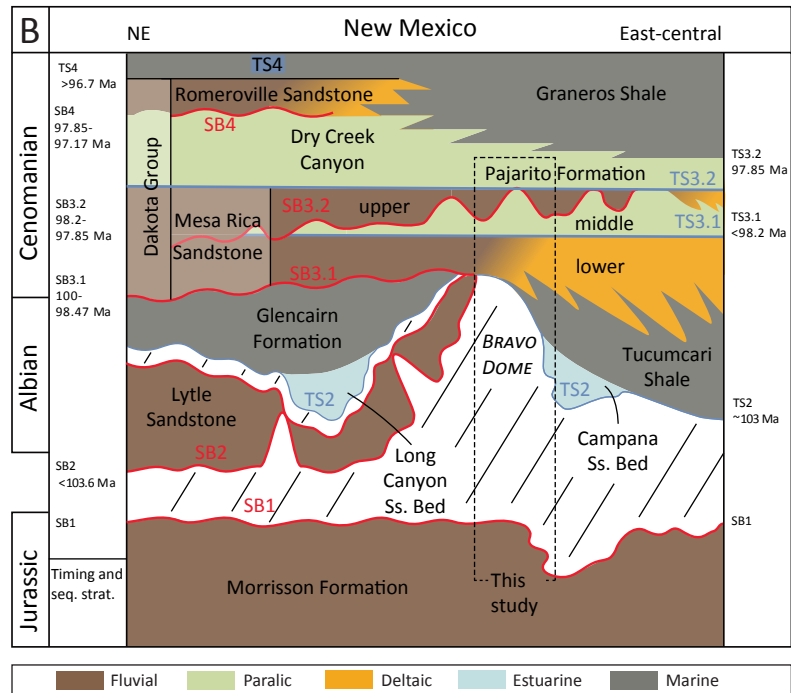
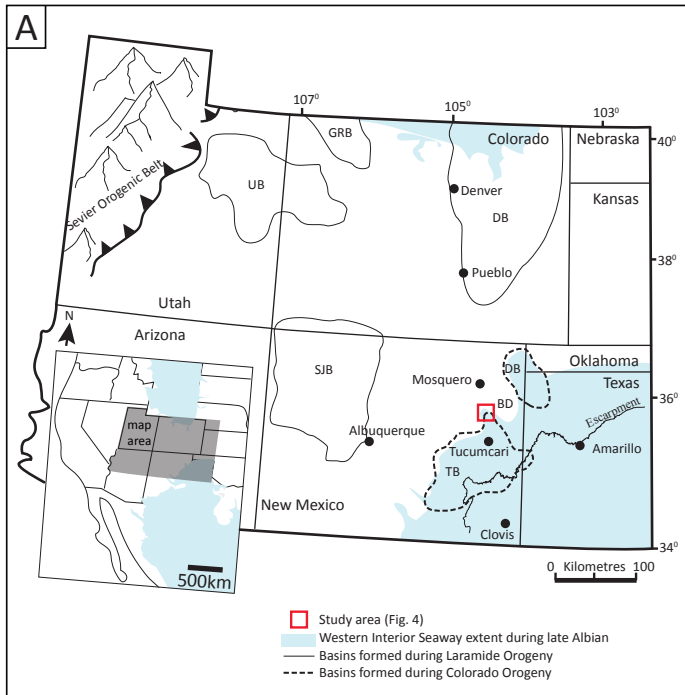
Mouth bar complex

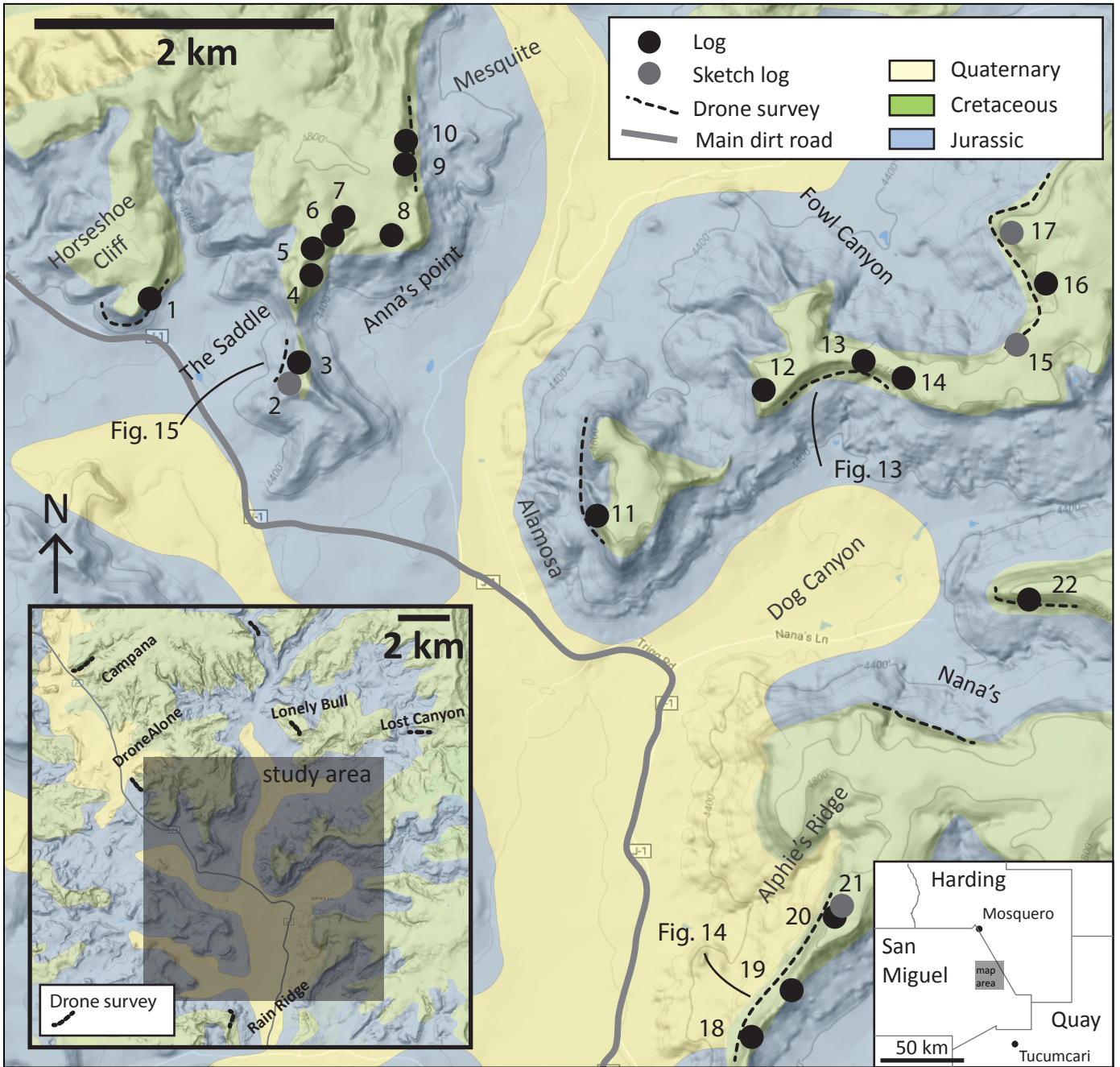
Delta lobe

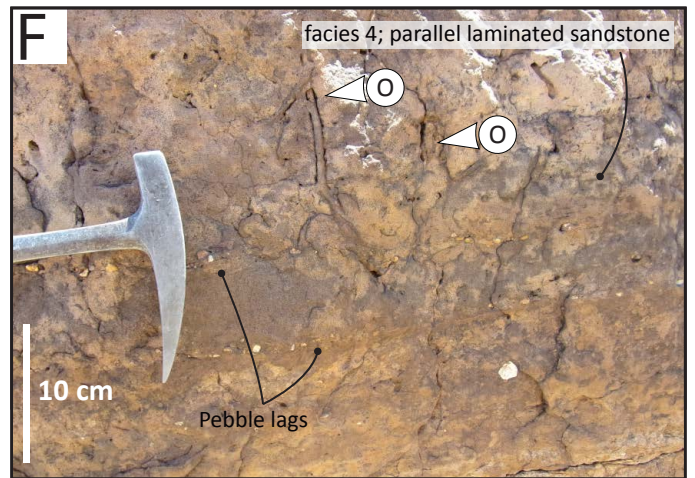
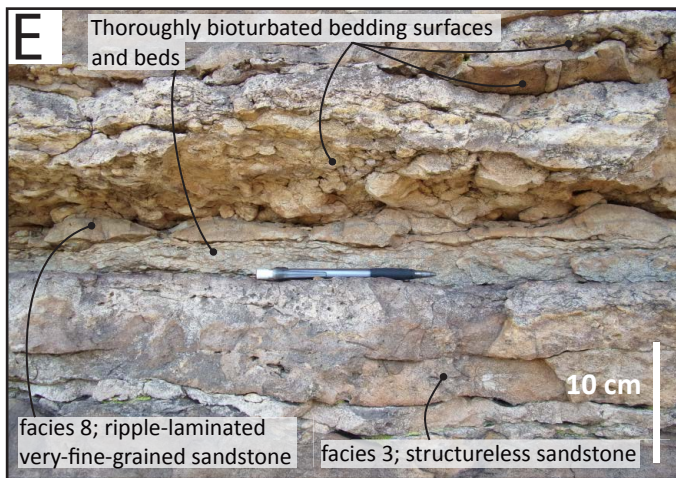
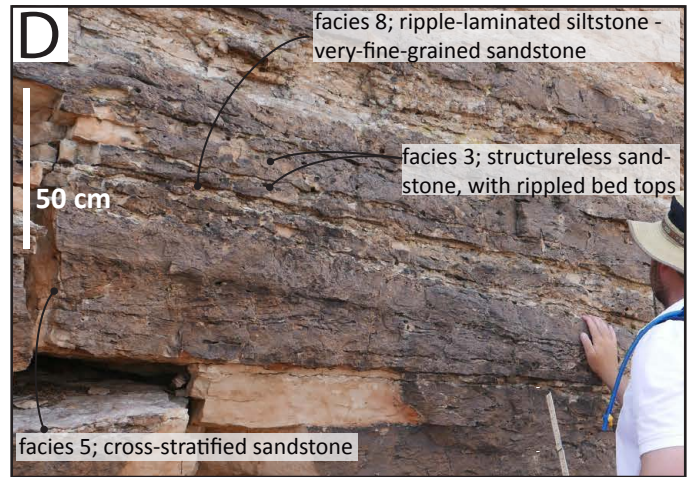
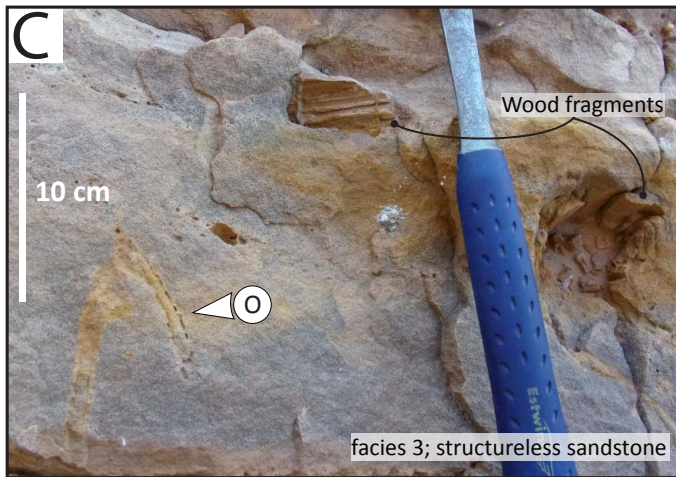
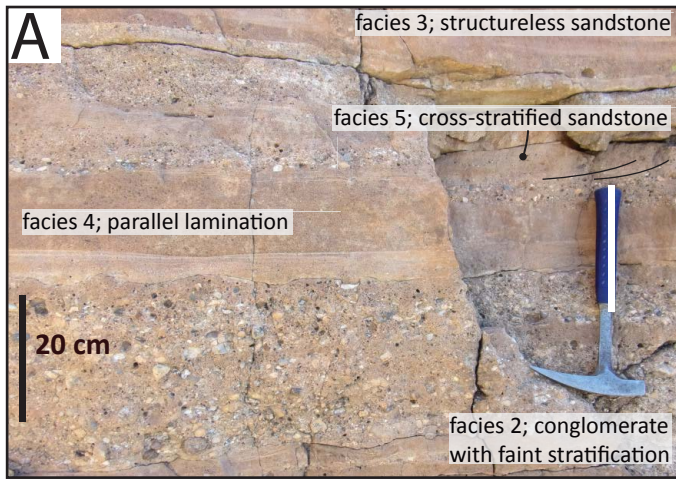
Delta system

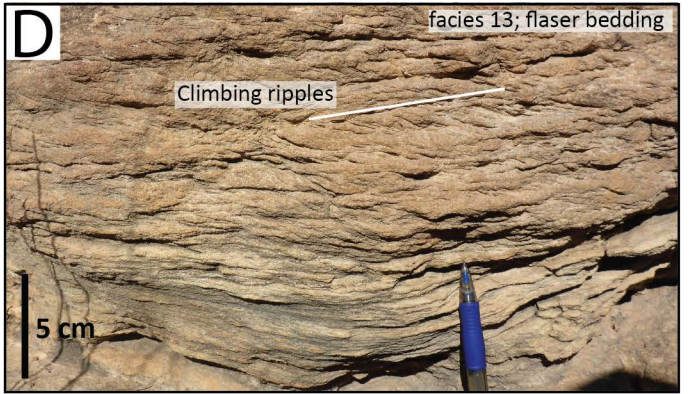
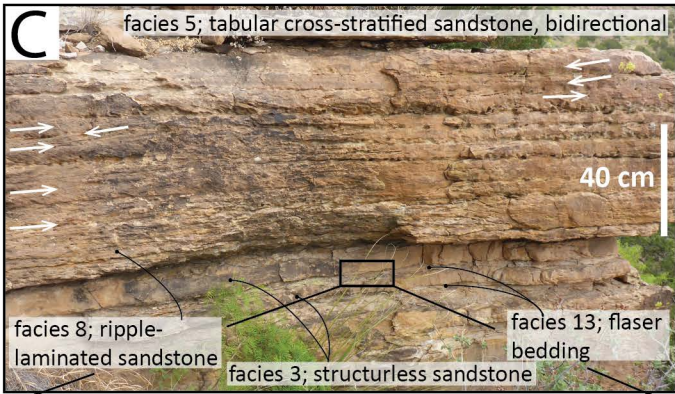
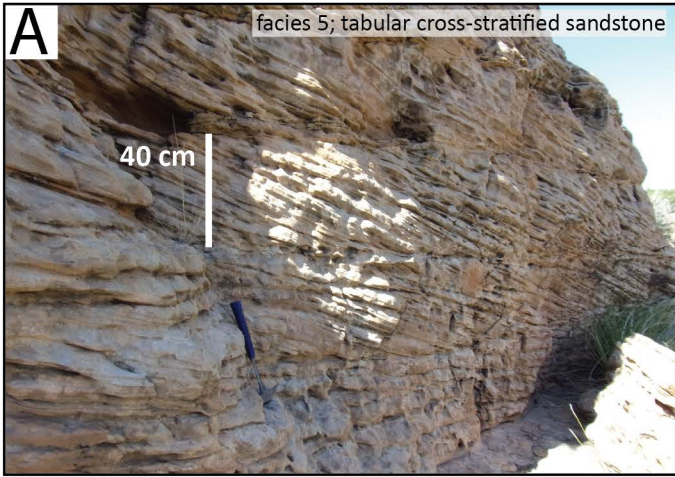


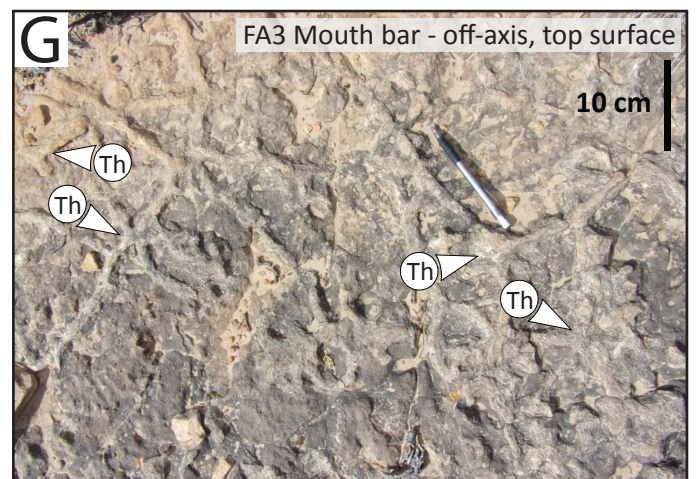
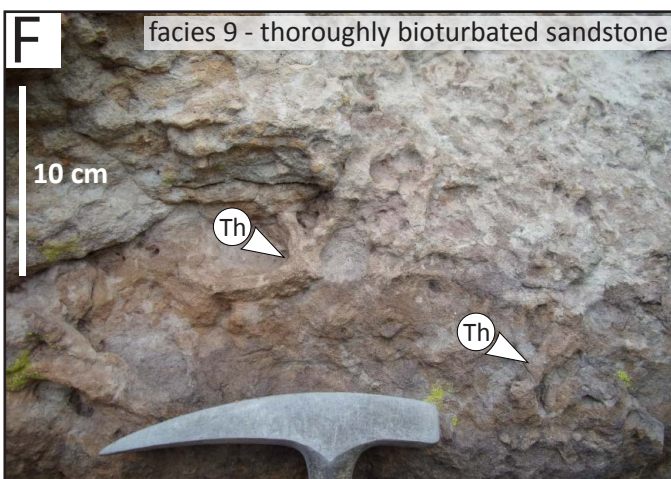
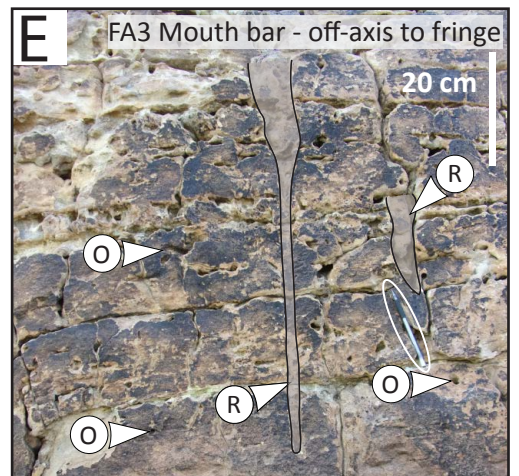
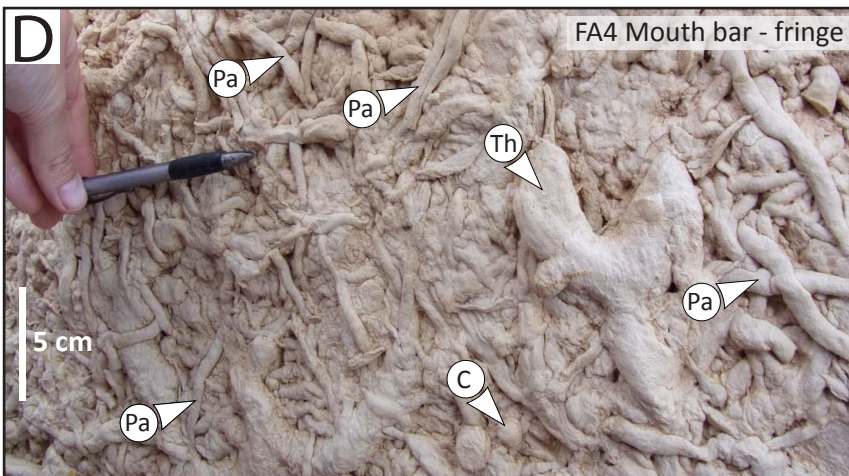
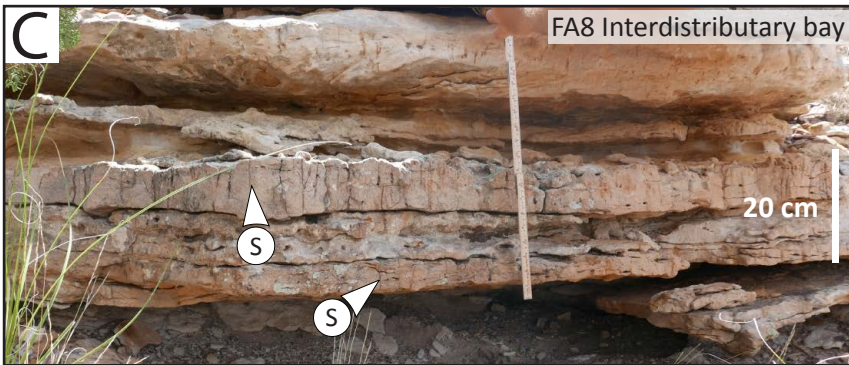
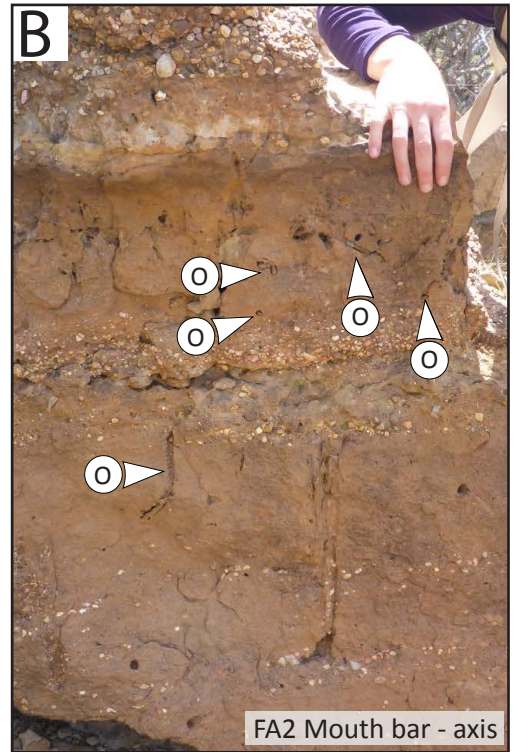
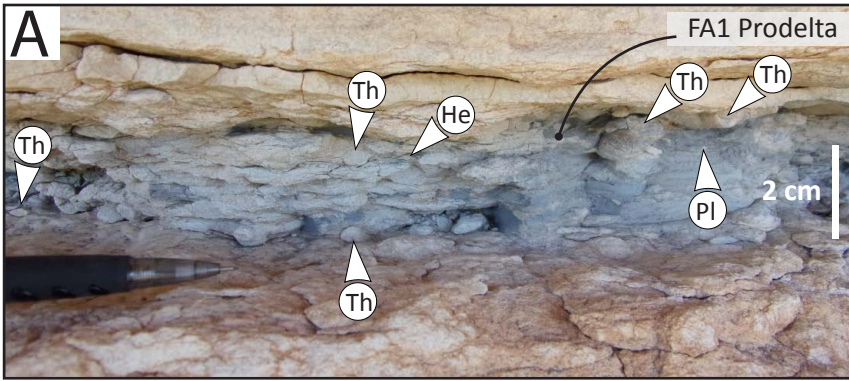
(Stream) mouth bar	Mouth bar complex / Bar assemblages	Delta lobe	Enge et al., 2010
Mouth bar	Mouth bar complex	Delta lobe	Kurcinka et al., 2018 Jerrett et al., 2018
Jet deposit	Jet deposit complex / Sub-lobe	Delta lobe	Wellner et al., 2005
Mouth bar element set	Mouth bar element complex	Element complex set	Ainsworth et al., 2016

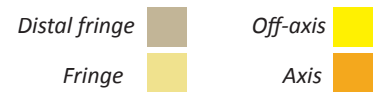
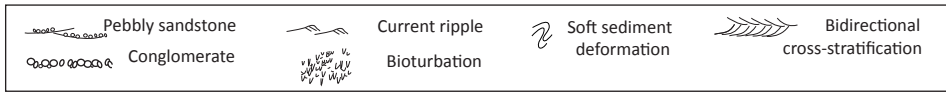
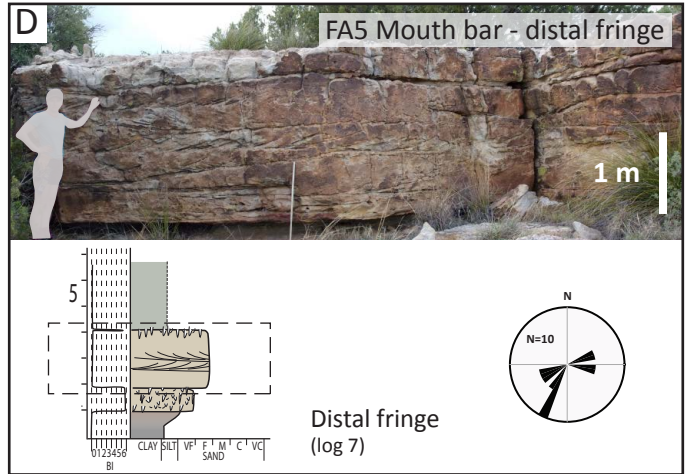
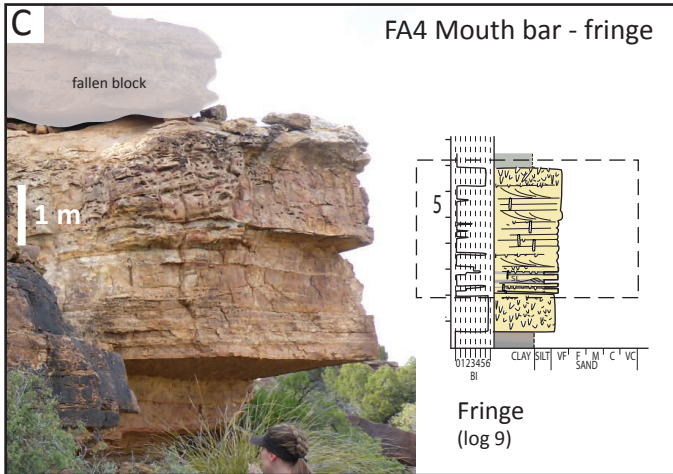
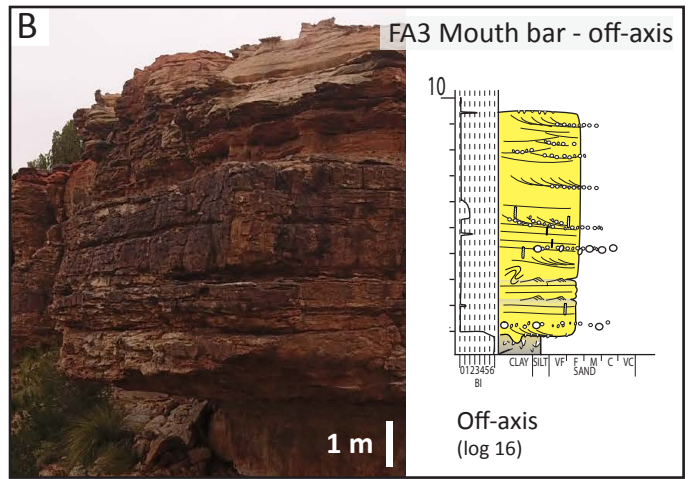
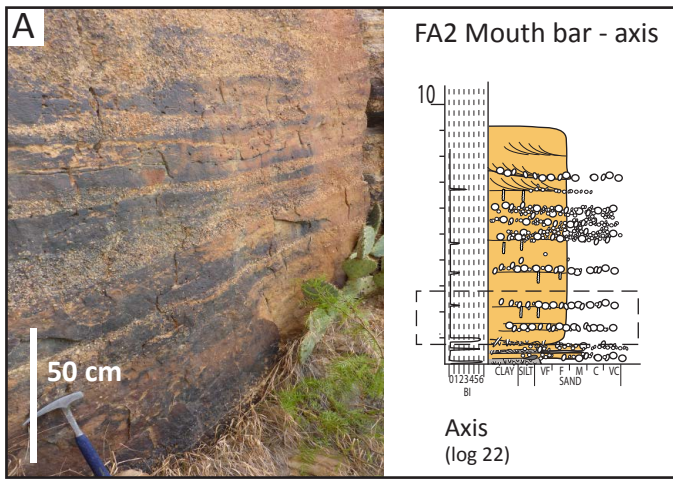


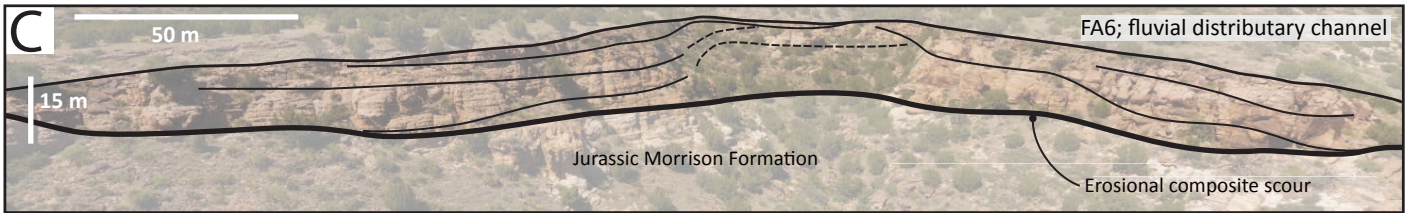
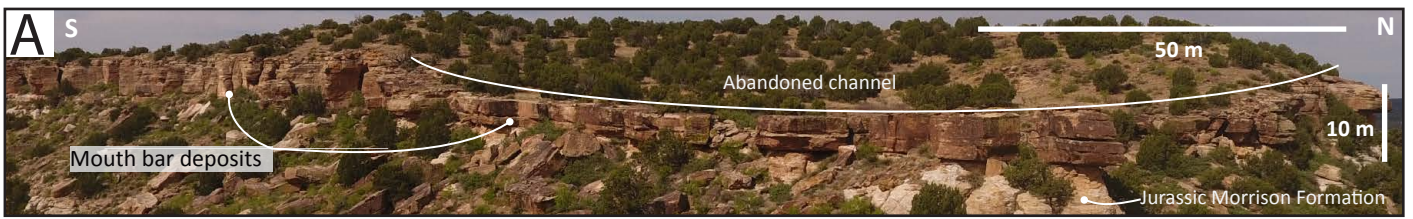


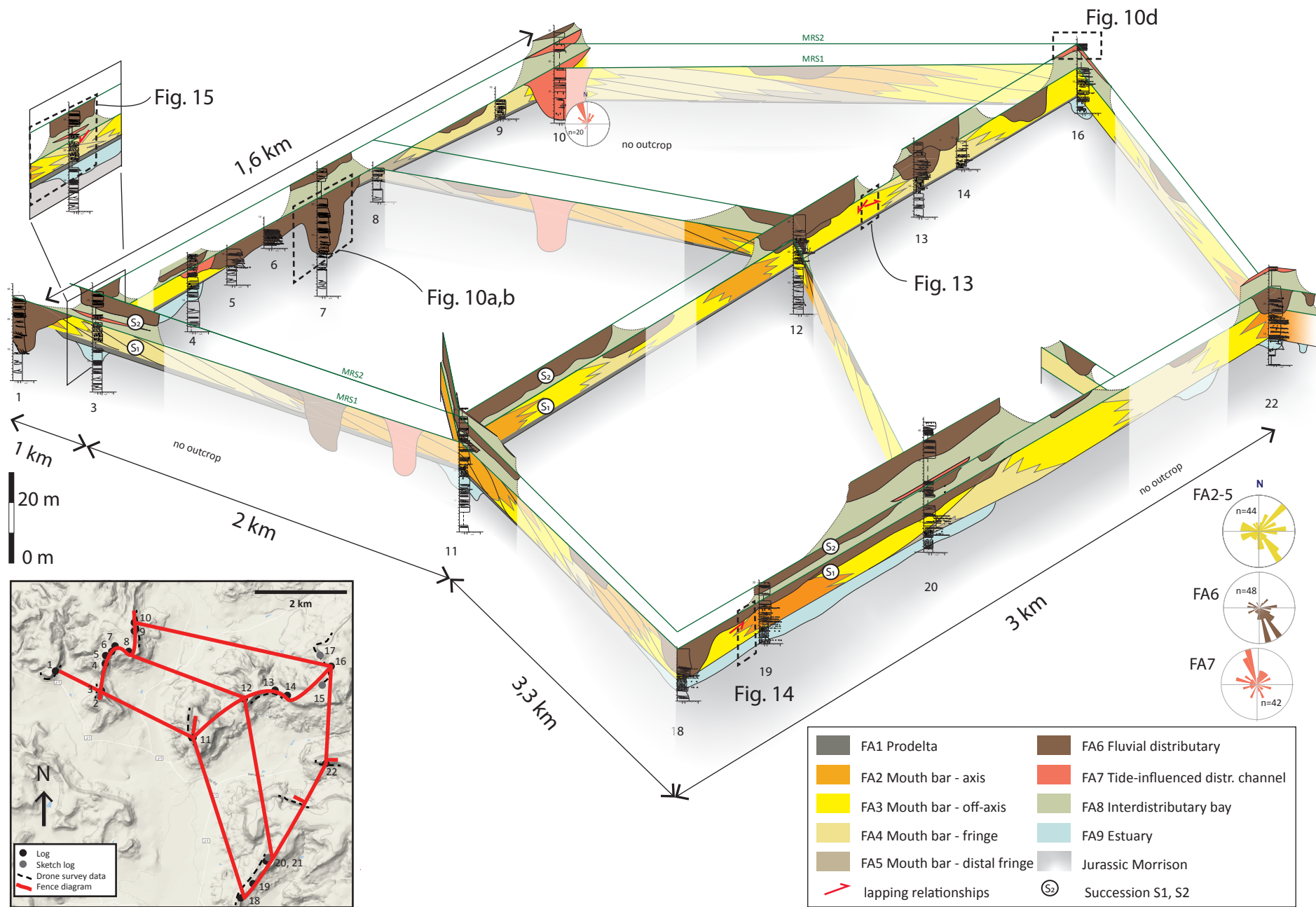


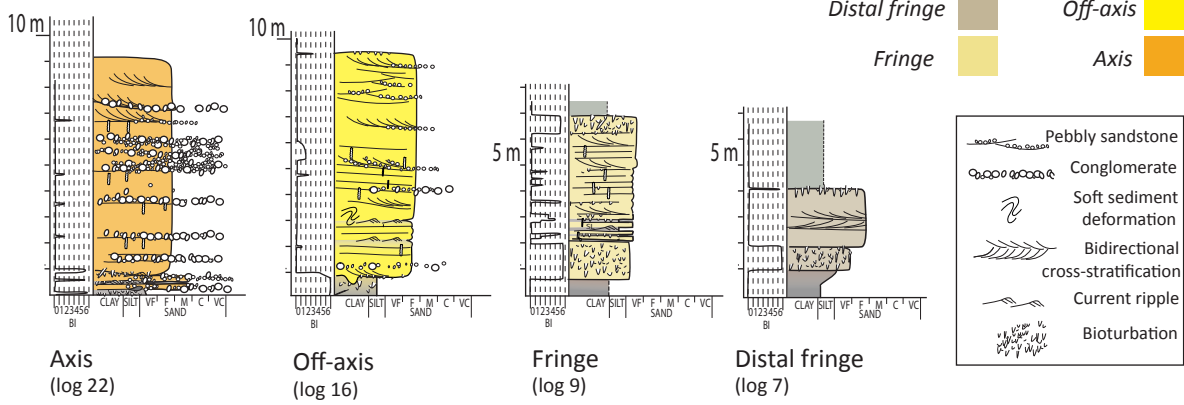
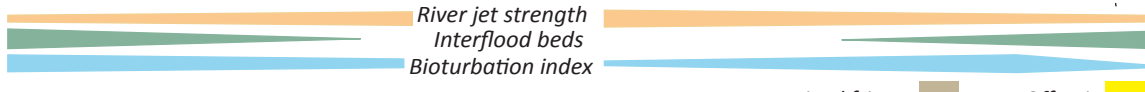
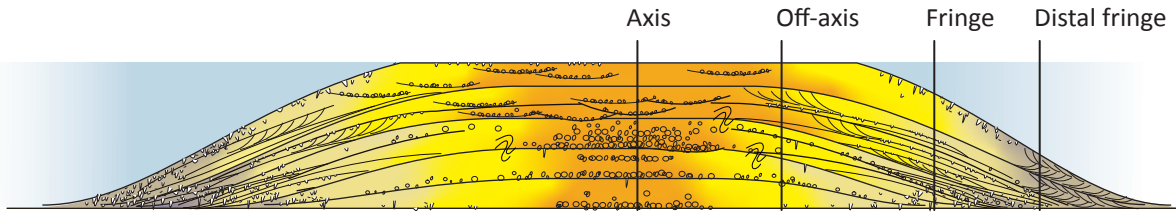










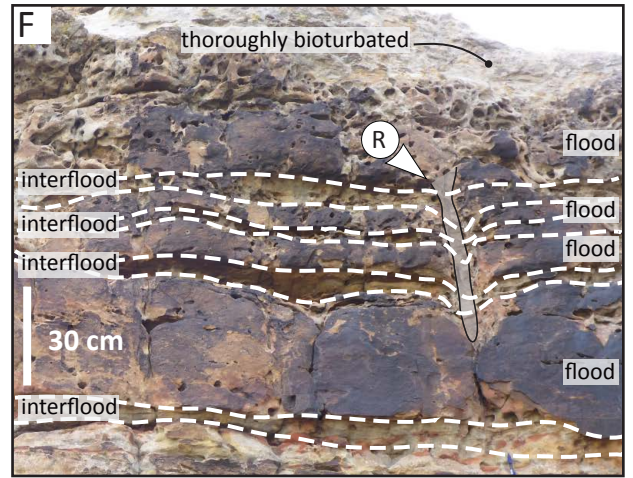
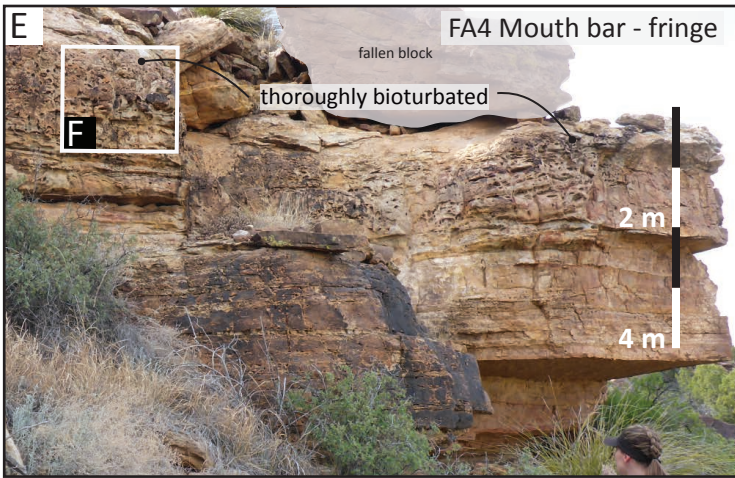
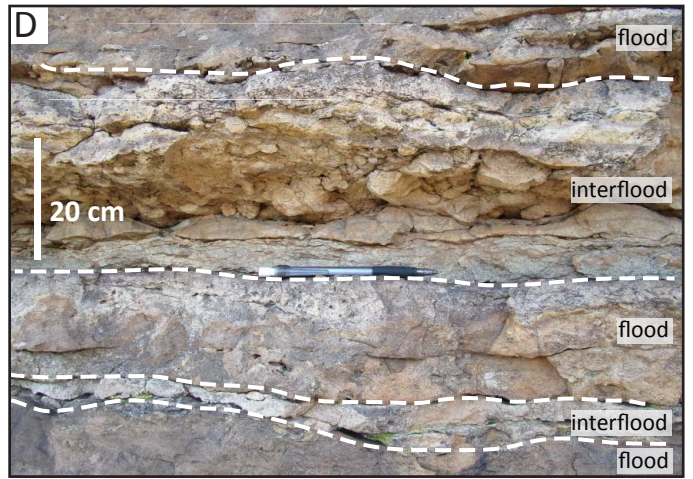
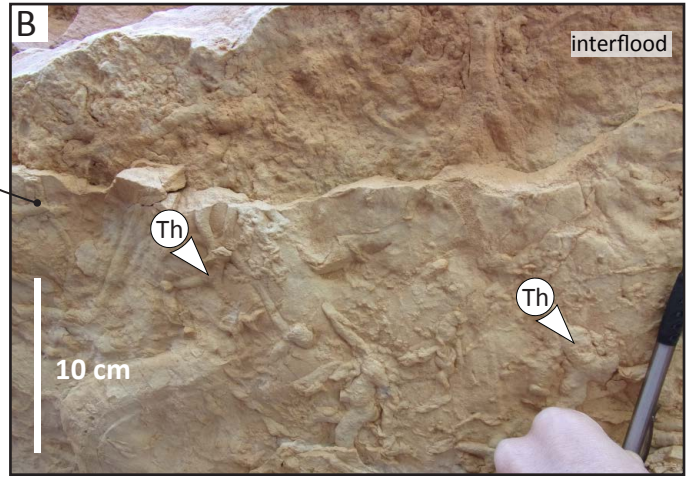
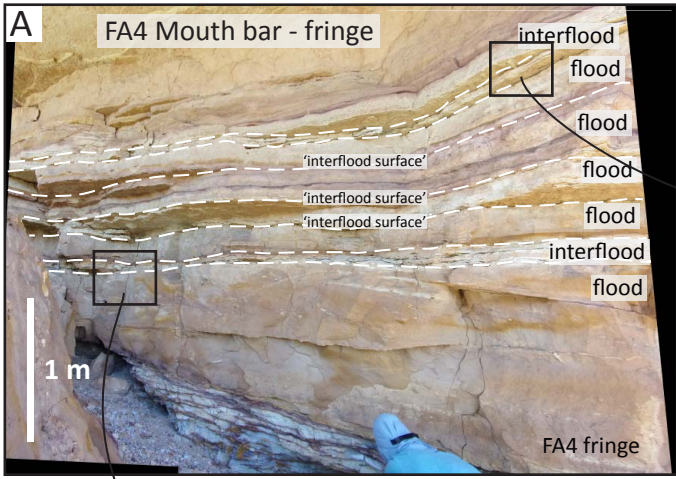


Axis
(log 22)

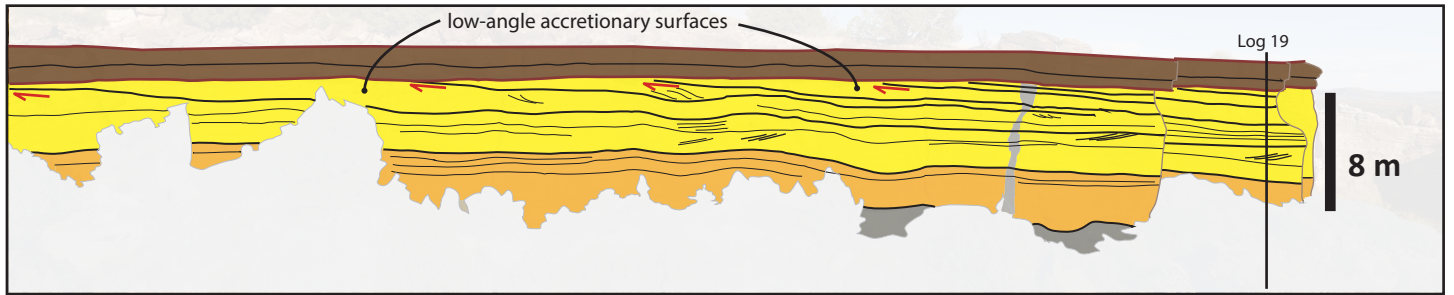
Off-axis
(log 16)

Fringe
(log 9)

Distal fringe
(log 7)







FA1 Prodelta FA2 Mouth bar - axis FA3 Mouth bar - off-axis FA6 Fluvial distributary channel

